nature reviews nephrology

https://doi.org/10.1038/s41581-025-00961-2

Review article

Check for updates

# Implantable bioelectronics and wearable sensors for kidney health and disease

Surabhi R. Madhvapathy[1,2,7], Soongwon Cho[1,7], Elisa Gessaroli[3,4,7], Eleonora Forte[4], Yirui Xiong[1,2], Lorenzo Gallon[4,8] ✉ & John A. Rogers[1,2,5,6,8] ✉

## Abstract

Established clinical practices for monitoring kidney health and disease — including biopsy and serum biomarker analysis — suffer from practical limitations in monitoring frequency and lack adequate sensitivity for early disease detection. Engineering advances in biosensors have led to the development of wearable and implantable systems for monitoring of kidney health. Non-invasive microfluidic systems have demonstrated utility in the detection of kidney-relevant biomarkers, such as creatinine, urea and electrolytes in peripheral body fluids such as sweat, interstitial fluid, tears and saliva. Implantable systems may aid the identification of early transplant rejection through analysis of organ temperature and perfusion, and enable real-time assessment of inflammation through the use of thermal sensors. These technologies enable continuous, real-time monitoring of kidney health, offering complementary information to standard clinical procedures to alert physicians of changes in kidney health for early intervention. In this Review, we explore devices for monitoring renal biomarkers in peripheral biofluids and discuss developments in implantable sensors for the direct measurement of the local, biophysical properties of kidney tissue. We also describe potential clinical applications, including monitoring of chronic kidney disease, acute kidney injury and allograft health.

## Sections



[1]Querrey Simpson Institute for Bioelectronics, Northwestern University, Evanston, IL, USA. [2]Department of Materials Science and Engineering, Northwestern University, Evanston, IL, USA. [3]Department of Medical and Surgical Sciences (DIMEC), Alma Mater Studiorum — University of Bologna, Bologna, Italy. [4]Department of Medicine, Division of Nephrology, University of Illinois College of Medicine, Chicago, IL, USA. [5]Department of Biomedical Engineering, Northwestern University, Evanston, IL, USA. [6]Department of Neurological Surgery, Northwestern University, Chicago, IL, USA. [7]These authors contributed equally: Surabhi R. Madhvapathy, Soongwon Cho, Elisa Gessaroli. [8]These authors jointly supervised this work: Lorenzo Gallon, John A. Rogers. ✉e-mail: Lgallon@uic.edu; jrogers@northwestern.edu

## Key points

- Advances in biosensors have led to the development of wearable and implantable systems for detecting indices of kidney health.
- Wearable biosensors are non-invasive alternatives to tests for biomarkers in blood, and include non-invasive microfluidic and microneedle-based systems with optical or electrochemical mechanisms to measure concentrations of kidney-relevant biomarkers in biofluids such as sweat, interstitial fluid, tears and saliva.
- Implantable devices enable direct measurements of the physical properties of the kidney, including tissue oxygenation, perfusion and temperature.
- Compared with blood tests and radiological procedures, these electronic devices enable the real-time capture of physiological data and may enable continuous monitoring over periods of time.
- Successful commercial translations of wearable biosensing devices are expected to benefit patients by reducing costs and providing invaluable real-time biochemical information for clinical decision making.
- Translational studies using large animal models with sufficiently large populations are needed to assess the predictive value of implantable biophysical sensors.

## Introduction

Kidney disorders affect more than 800 million people worldwide and are a leading cause of morbidity and mortality[1]. These disorders are characterized by kidney damage resulting from various conditions, including diabetes, hypertension, autoimmune diseases, genetic factors, aging, and infections[2]. Damaged kidneys have impaired functionality and blood-filtering capabilities, resulting in the improper discarding of waste products and excess fluids that worsen organ damage. If not treated, these disorders eventually lead to organ failure and the need for kidney replacement therapy. Screening for risk factors, early diagnosis and monitoring of disease progression and response to treatment are critical to prevent and/or mitigate organ damage and guide targeted interventions. Early intervention is also imperative to increase life quality and expectancy of patients with kidney diseases.

Chronic kidney disease (CKD) and acute kidney injury (AKI) are the most prevalent kidney disorders, affecting 700 million and 13 million people globally, respectively[1]. CKD occurs when the organ is subject to damage for a period >3 months and is often driven by diabetes and hypertension[2]. AKI is of short duration, marked by an abrupt decline in organ function or severe kidney injury, and often develops in critically ill patients[3]. AKI sequelae can progress to CKD or kidney failure.

Kidney transplantation is the treatment of choice for patients with kidney failure, leading to better quality of life and longer life expectancy than dialysis[4]. Unfortunately, long-term organ and patient survival rates remain unsatisfactory, with ~50% of transplant recipients experiencing graft failure at 10 years post-transplantation and mortality of >30%[4–6]. Diagnostic biomarkers of allograft dysfunction and rejection are therefore crucial to facilitate early intervention and improve transplant outcomes.

Standard diagnostics of kidney disorders rely on a combination of tests, including blood and urine analyses, diagnostic imaging and kidney biopsies. Blood tests that are traditionally used for assessing kidney function generally rely on the measurement of waste products of the blood filtration process. Serum creatinine is the most commonly used marker, but it can be influenced by several factors that are independent of kidney disease and often demonstrates a delayed response to AKI. Relying solely on this parameter can limit the detection of subclinical kidney damage[7,8].

Other traditionally recognized biomarkers of kidney dysfunction include blood urea nitrogen (BUN), proteinuria and albuminuria, which are monitored in patients with native kidney disease and in transplant recipients[9–11]. However, their sensitivity and specificity as biomarkers of kidney injury are study- and disease-dependent (Supplementary Table 1). Novel blood and urinary biomarkers have demonstrated the potential to improve the management of allograft dysfunction and rejection in transplant recipients[12] (Supplementary Table 2); however, multicentre validation studies are necessary to define their utility and application in clinical practice[13].

In addition to serological and urine tests, several common radiological tools can aid assessments of kidney injury, such as ultrasonography (including Doppler ultrasound and contrast-enhanced ultrasound (CEUS)), CT and MRI (Supplementary Table 3). Despite current technological advances, these tools have several limitations in detecting AKI and/or CKD, and their overall specificity and sensitivity for the diagnosis of kidney disease are not completely defined[14–17].

In the context of abnormal urinary findings or acute deterioration of kidney function, clinicians routinely perform percutaneous ultrasound-guided kidney biopsies for diagnostic and prognostic purposes[18,19]. Histological analysis of native kidney and transplant biopsy samples provides valuable information and is widely used to guide therapeutic decision making[18,19]. However, percutaneous biopsies are costly, invasive and can potentially lead to complications such as pain and bleeding[20]. Thus, they cannot be easily used for screening and monitoring purposes.

Overall, the available diagnostic techniques are suboptimal because they lack sensitivity and specificity, can trigger complications and delay diagnosis, thereby preventing early treatment that could limit disease progression. Alternative, non-invasive, cost-effective and easily measurable clinical biomarkers of kidney damage are therefore needed. Ideal biomarkers should have high sensitivity and specificity for different kidney diseases and relative stages; identify the outset of kidney injury and its underlying causes; monitor disease progression and response to treatment; and have diagnostic, prognostic or predictive value[21].

This Review highlights the utility of bioelectronic devices[22–26] as promising alternatives to traditional physiological assessments of kidney health. Compared with blood tests and radiological procedures, these electronic devices enable the real-time capture of physiological data without the need for expensive, time-consuming procedures and frequent hospital visits. We first explore wearable, non-invasive sensors for the detection of renal biomarkers in peripheral biofluids such as sweat, interstitial fluid, tears and saliva. The following sections investigate implantable devices for direct measurements of the physical properties of the kidney, including tissue oxygenation, perfusion and temperature.

## Wearable, non-invasive biochemical sensors

Analysis of biomarkers in blood represents the clinical standard for determining kidney dysfunction. This process involves the collection

of relatively large volumes of blood (1–3 ml) by trained health care professionals in hospital settings, usually through invasive venipuncture, and evaluation of the collected samples with complex, expensive laboratory analytical systems[27,28]. These procedures impose practical limitations on the frequency of such assessments, typically with long delays between the blood draws and receipt of results. Such analyses therefore remain reactive and episodic, and lack the ability to rapidly track changes in biomarker concentrations for early detection of disease.

Both AKI and CKD can be asymptomatic or present with minimal symptoms, which often delays diagnosis and timely therapeutic intervention[29]. Non-invasive, real-time monitoring of kidney function could enable early disease detection and monitoring of disease progression, thus facilitating timely hospitalization and prompt therapeutic intervention. Furthermore, a wearable monitoring system could improve the quality of life of patients with kidney disease by minimizing the need for frequent hospital visits to perform blood draws. This approach offers great value for individuals at a high risk of disease progression who require close medical supervision. In addition, such an approach could improve the prescription and management of nephrotoxic drugs that are prescribed by different specialties, including oncology, haematology, nephrology and cardiology, thereby enabling clinicians to make precise therapeutic dose adjustments on the basis of kidney function.

Kidneys are essential for regulating and maintaining several homeostatic processes, including hydro-electrolyte equilibrium. Non-invasive continuous monitoring of electrolytes (for example, $K^+$, $Na^+$, $Ca^{2+}$ and $Mg^{2+}$) could enable early detection of metabolic imbalances. Dyskalaemias, dysnatraemias and dysmagnesaemias are examples of common electrolyte disorders that can lead to serious complications, sometimes requiring immediate medical intervention[30]. Traditional blood tests offer only a snapshot of electrolyte levels at a specific moment, and potentially miss critical fluctuations that occur between measurements and during dialysis sessions. Continuous monitoring could also enable early detection of abnormal trends, allowing clinicians to make timely therapeutic adjustments and prevent severe complications.

Peripheral biofluids, such as sweat, interstitial fluid (ISF), saliva and tears, contain appreciable concentrations of kidney-relevant biomarkers, including glucose, creatinine, urea, uric acid, cystatin C and electrolytes[31,32]. Wearable sensors that can evaluate these species in biofluids may serve as fast, non-invasive alternatives to traditional blood analysis (Table 1, Fig. 1). Available approaches use optical and electrochemical[27,33] mechanisms to sense these biomarkers (Table 2). Electrochemical biosensors use amperometric, potentiometric and impedance-based techniques, often paired with wireless systems for data transfer. Optical biosensors commonly operate based on digital images of colorimetric or fluorometric responses to target analytes. Future efforts will be aimed at establishing capabilities for continuous monitoring of these species, with the goal of improving patient care.

## Sweat

Eccrine sweat is secreted by glands that are distributed across nearly all regions of the human epidermis and has an essential role in thermal regulation[34]. Sweat also contains many biochemical species, including those relevant to kidney health[27,28] (Table 2). The most versatile approaches for evaluating kidney-relevant biomarkers in sweat use soft, skin-interfaced microfluidic systems[23,35–40]. These devices route pristine, microlitre volumes of sweat as it emerges from the surface of the skin through collections of microfluidic channels, valves and reservoirs to detect biomarker concentrations in real time. Additional capabilities include wireless transmission of this information to users through standard portable devices such as smartphones.

### Relevance of sweat for kidney disease

Motivation for the development of sweat analytic systems for renal monitoring arose from exploratory clinical studies of sweat collected from patients with kidney failure[41–43]. A 1997 study reported concentrations

**Table 1 | Biomarker concentrations for healthy individuals and patients with kidney disease**

| Subject | Target biomarker | Blood | Sweat | ISF | Tears | Saliva |
|---|---|---|---|---|---|---|
| Healthy individuals | Creatinine | 61–124 μM[169] | 5–15 μM[35,47,48a] | 50–100 μM[27,170] | 50–125 μM[81] | 4–18 μM[27,171] |
| | Urea | 1.2–7.1 mM[56,169] | 2–15 mM[35] | 4–6 mM[172] | 3–7.5 mM[81] | 2–11.67 mM[27,171] |
| | Uric acid | 100–200 μM[42] | 29–51 μM[42]<br>10–35 μM[56] | NA | 30–420 μM[173] | 50–450 μM[109] |
| | Sodium | 135–148 mM[169] | 20–100 mM[174] | 135–150 mM[175] | 120–170 mM[176] | 6.1–217 mM[111,112] |
| | Potassium | 3.5–5.0 mM[169] | 3.3–7.3 mM[57] | 3.8–4.9 mM[175] | 26–42 mM[176] | 2.6–18.3 mM[109,112] |
| | Chloride | 95–105 mM[169] | 10–40 mM[177] | 99–117 mM[175] | 120–135 mM[176] | 6–35 mM[178] |
| Patients with kidney failure prior to dialysis | Creatinine | 509–854 μM[43] | 23–50 μM[43] | NA | 130–430 μM[81] | 40–127 μM[43] |
| | Urea | 19–26 mM[43] | 22–33 mM[43] | 16–36 mM[65] | 6.8–27 mM[81] | 21–30 mM[43] |
| | Uric acid | 460–780 μM[42]<br>110–400 μM[41] | 65–139 μM[42]<br>20–60 μM[41] | NA | NA | 140–480 μM[109]<br>823 μM[106] |
| Patients with kidney failure post-dialysis | Creatinine | 145–275 μM[43] | 17.2–27.3 μM[43] | NA | 50–280 μM[81] | 10.5–25.7 μM[43] |
| | Urea | 4.1–7.6 mM[43] | 9.1–15.1 mM[43] | 6.3–15.6 mM[65] | 3.8–16.0 mM[81] | 4.1–7.5 mM[43] |
| | Uric acid | 60–240 μM[109] | NA | NA | NA | 60–220 μM[109] |

ISF, interstitial fluid; NA, not available. [a]Measured in the absence of stress.

of urea in sweat from 11 female patients with kidney failure[41], captured in volumes of 1–1.5 ml from the chin regions using plastic disposable syringes following thermally induced activation of eccrine glands. Spectroscopic quantification of biomarker concentrations using a diacetyl monoxime colorimetric method[41] indicated that urea concentrations were 2–15-fold higher in patients with kidney failure[41] than in healthy individuals[44]. These initial results supported the relevance of sweat-based analytics in patients with kidney disease.

A more recent study[43] examined concentrations of urea and creatinine in the sweat of 40 patients with kidney failure. Sweating was induced by passing pilocarpine through the skin of the forearm by iontophoresis. Sweat was collected using a commercial system and analysed using spectrometry based on commercial enzymatic reagent kits via optical absorbance. For example, the urea quantification kit uses an NADH–glutamate dehydrogenase coupled reaction system, where the rate of decrease in chromogenic concentrations of NADH is dependent on the urea concentration. In the creatinine kit, creatininase, creatinase and sarcosine oxidase liberate hydrogen peroxide, which then reacts with 4-aminophenazone and 2,4,6-triiodo-3-hydroxybenzoic acid (HTIB) to produce a quinone imine chromogen, which can be measured. The findings from that study indicated that concentrations of urea and creatinine in sweat correlate with those in serum and saliva, validating

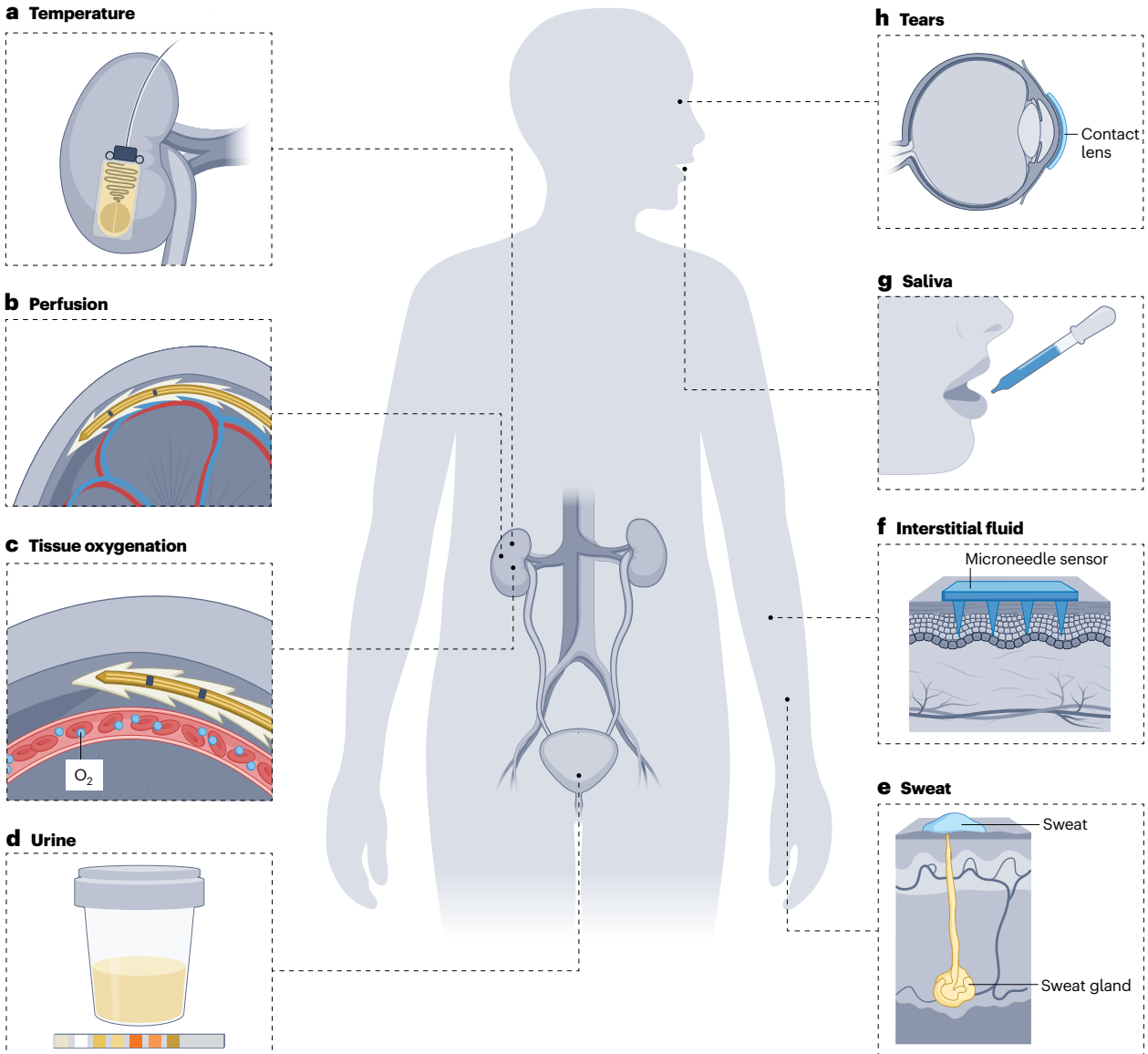


**Fig. 1 | Bioelectronic devices for monitoring kidney health. a**, Soft, flexible, fully implantable sensors enable the detection of temperature changes for early detection of kidney transplant rejection. **b**, Wireless, self-fixing thermal sensors can be used to monitor microvascular perfusion on the surface of the perfused kidney. **c**, Wireless optical sensors can monitor oxygenation within kidney as a measure of perfusion. **d**, Sample collection and test strips are commonly used to detect key biomarkers of kidney function in urine. **e**, Wearable, soft, skin-interfaced microfluidic devices can be used to sense kidney biomarkers in sweat. **f**, Wearable microneedle-based continuous sensors can be used to sense kidney biomarkers in interstitial fluid. **g**, Saliva can also be used as a biofluid for detection of renal biomarkers. **h**, Wearable smart contact lenses and other devices could be used to detect renal biomarkers in tears.

**Table 2 | Wearable devices for monitoring of kidney health**

| Bio- fluid | Target analyte | Concentration in biofluid | Linear range (LOD) | Recognition element | Transducer | Technique | Mode | Ref. |
|---|---|---|---|---|---|---|---|---|
| Sweat | Creatinine | 9–15 μM | 10–500 μM (NA) | Creatinase, creatininase, sarcosine oxidase | Creatinine probe | Colorimetry | Multi-point | 35 |
| | Urea | 2–15 mM | 10–250 mM (NA) | Urease | pH paper | | | |
| | Creatinine | N/A | 12–40 ng (12 ng) | Silver nanoflakes | Raman scattering | Surface-enhanced Raman spectroscopy | Multi-point | 46 |
| | Creatinine | 5–65 μM | 0.4–960 μM (0.06 μM) | Cuprous oxide nanoparticle | PVA–carbon black–$Cu^{2+}$–PEDOT:PSS | Electrochemical impedance spectroscopy | Continuous | 47 |
| | Creatinine | 10–40 μM | 0.6–2,800 μM (0.12 μM) | GO-Cu(II)/Cu-BDC MOF/$Cu_2O$ NPs | $Na^+$-doped carbon–PEG/PPy/$Ti_3C_2T_x$ | Amperometry | Continuous | 48 |
| | Urea | N/A | 30–180 mM (30 mM) | Urease | Phenol red on cotton | Colorimetry | Single point | 51 |
| | Urea | 13–30 mM | 1–100 mM (0.1 mM) | Surface molecular imprinted nanotube | Carbon nanotube/ potassium ferricyanide | Amperometry | Single point | 54 |
| | Urea | 17.5 mM | 0.9–50 mM (0.4 mM) | Urease | Cholesteric LC in poly(acrylic) acid | Colorimetry | Single point | 50 |
| | Urea | 10.9 mM | 5–200 mM (5 mM) | Urease | PANI ink on electrode | Potentiometry | Continuous | 53 |
| | Uric acid | 5–130 μM | 0.74–200 μM (0.74 μM) | Laser-engraved graphene | Laser-engraved graphene | Amperometry | Multi-point | 42 |
| | Uric acid | 40–65 μM | 2–250 μM (1.2 μM) | PEDOT:PSS hydrogel | PEDOT:PSS hydrogel on carbon screen-printed electrode | Amperometry | Continuous | 55 |
| | Potassium | 3.3–7.3 mM | 0.1–100 mM (0.1 mM) | Valinomycin, KTCPB, PVC, DOS | Poly(3-octyl thiophene-2,5-diyl) | Potentiometry | Continuous | 57 |
| ISF | Creatinine | 45–150 μM (mouse) | 50–550 μM (18 μM) | Creatininase, creatinase sarcosine oxidase | Prussian blue on carbon screen-printed electrode | Amperometry Potentiometry | Single point | 69 |
| | Uric acid | 80–260 μM (mouse) | 50–550 μM (31 μM) | Uricase | | | | |
| | Urea | 4–10 mM (mouse) | 1–16 mM (0.49 mM) | Urease | Ammonium ionophore, PVC-COOH, DOS on screen-printed carbon | | | |
| | Urea | 4.5–10 mM (mouse) | 3–18 mM (0.9 mM) | Urease | Au microneedle with urease and Nafion | Potentiometry | Continuous | 70 |
| | Urea | N/A | 0.05–2.5 mM (0.0028 mM) | Urease | Au nanoparticle ink with organic polymer | Amperometry | Continuous | 179 |
| | Potassium | N/A | 0.063–79 mM (0.012 mM) | Valinomycin, KTCIPB, PU, DOS | Carbon coated with functionalized MWCNTs | Potentiometry | Continuous | 72 |
| | Cystatin C | NA | 38.5–385 nM | Anti-cystatin C antibody | Lateral flow assay | Colorimetry | Single point | 180 |
| Tears | Creatinine | 85–130 μM | 1.6–2,400 μM (0.8 μM) | GO-Cu(II)/Cu-BDC MOF/$Cu_2O$ NPs | Cotton fibre-based carbon black | Amperometry | Continuous | 95 |
| | Urea | N/A | 0.08–2.5 mM (0.078 mM) | Orthophthaldialdedyde | Primaquine diphosphate | Colorimetry | Single point | 84 |
| | Uric acid | N/A | 0.3–1.5 mM (0.3 mM) | Uricase | 4-AMP, HRP | Colorimetry | Single point | 87 |
| | Potassium | N/A | 3–50 mM (3 mM) | DA18C6 chelation (crown ether) | DA18C6 (crown ether) | Fluorometry | Single point | 100 |
| Saliva | Uric acid | 175–816 μM | 200–1,000 μM (200 μM) | Uricase | Prussian blue | Amperometry | Continuous | 106 |
| | Potassium | 4.2–5.2 mM | 1–100 mM (1 mM) | Valinomycin, KTFPB, PVC, DOS | Ag electrode | Potentiometry | Continuous | 107 |

BDC, benzene dicarboxylate; DOS, bis(2-ethylhexyl)sebacate; HRP, horseradish peroxidase; KTCPB, potassium tetrakis(4-chlorophenyl) borate; LC, liquid crystal; LOD, limit of detection; MOF, metallo-organic framework; MWCNTs, multiwalled carbon nanotubes; NA, not available; NPs, nanoparticles; PANI, polyaniline ink; PEDOT:PSS, poly(3,4-ethylenedioxythiophene):polystyrene sulfonate; PEG, polyethylene glycol; PU, polyurethane; PVA, polyvinyl alcohol.

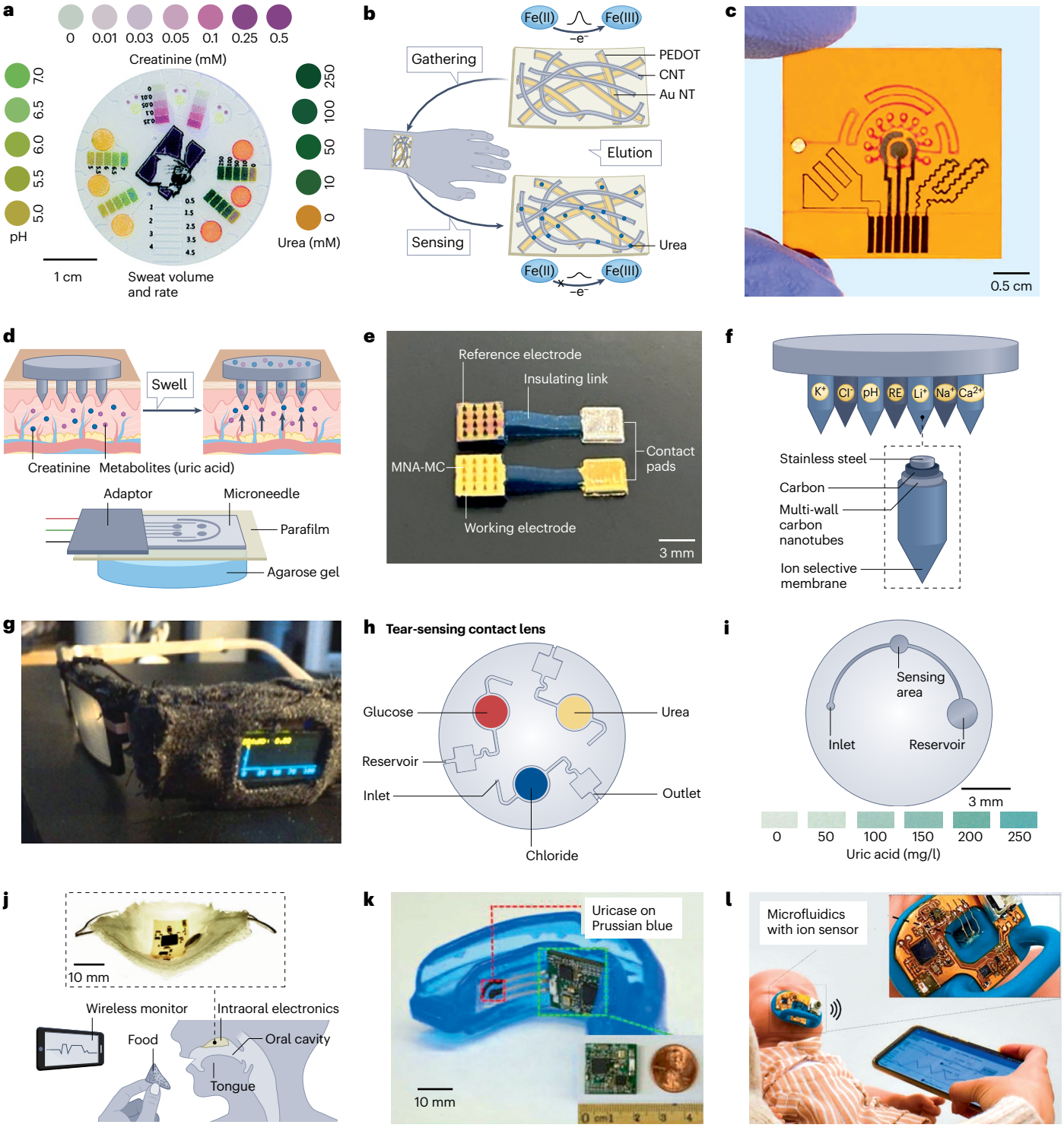


the relevance of these biofluids for patient diagnostics[43]. This study[43] further shows that after haemodialysis, concentrations of urea and creatinine in sweat decrease in a similar manner to their respective values in plasma.

Advances in bioengineering have also demonstrated the ability of skin-interfaced microfluidic devices to monitor concentrations of uric acid in sweat[42]. These soft, flexible devices attach to the forehead to route sweat induced by physical exercise to microfluidic chambers for potentiometric detection of uric acid[42]. One study of 15 individuals revealed differences in uric acid concentrations between healthy individuals, those with gout and those with hyperuricaemia (40 μM, 100 μM and 78 μM, respectively)[42]. Data also indicated that

**Fig. 2 | Wearable biochemical monitoring of kidney health. a**, Optical image of a soft microfluidic system for colorimetric analysis of sweat biomarkers relevant to kidney disorders including creatinine, urea and pH. (Part **a** is reprinted with permission from ref. 35, Royal Society of Chemistry.) **b**, Schematic image of the surface of a molecularly imprinted poly(3,4-ethylenedioxythiophene) (PEDOT) polymer on carbon nanotubes (CNT) and gold nanotubes (Au NT) for monitoring sweat urea. (Part **b** is adapted with permission from ref. 54, ACS Publications.) **c**, Optical image of a differential pulse voltametric electrochemical sweat sensor for detecting uric acid and tyrosine. (Part **c** is reprinted from ref. 42, Springer Nature Limited.) **d**, Schematic of rapidly swellable microneedle array for efficient extraction of interstitial fluid (ISF) and testing setup with Parafilm and agarose gel for benchtop evaluation of creatinine and uric acid in ISF. (Part **d** is adapted with permission from ref. 69, Elsevier.) **e**, Optical image of a microneedle with microcavities for transdermal electrochemical monitoring of urea in ISF. Microcavities are used to accommodate the sensing layer and provide protection from mechanical delamination during skin insertion or removal. (Part **e** is reprinted with permission from ref. 70, ACS Publications.) **f**, Schematic of a microneedle array for detection of pH and multiple electrolytes in ISF, including $K^+$, $Cl^-$, $Na^+$, $Li^+$, $Ca^{2+}$. (Part **f** is adapted from ref. 76, CC BY 4.0 (https://creativecommons.org/licenses/by/4.0/).) **g**, Optical image of a lab-on-eyeglass for sensing of creatinine in tears. (Part **g** is reprinted with permission from ref. 95, ACS Publications.) **h**, Schematic of a smart contact lens for monitoring of tear biomarkers, including urea, glucose and chloride. (Part **h** is reprinted from ref. 84, Springer Nature Limited.) **i**, Optical image of a femtosecond laser-written microfluidic lens for colorimetric uric acid sensing in tears. (Part **i** is reprinted with permission from ref. 87, Wiley.) **j**, Optical images and conceptualization of intra-oral dental retainer for saliva glucose monitoring. (Part **j** is adapted with permission from ref. 104, National Academy of Sciences.) **k**, Optical image of a mouthguard for detection of uric acid in saliva. (Part **k** is reprinted with permission from ref. 106, Elsevier.) **l**, Optical image of a smart bioelectronic pacifier for real-time continuous monitoring of salivary electrolytes. (Part **l** is reprinted with permission from ref. 107, Elsevier.). MNA-MC, microneedle arrays–microcavities; RE, reference electrode.

concentrations of uric acid in sweat correlated strongly with those in serum[42].

Positive correlations between creatinine, urea and uric acid levels in sweat with those in blood clearly establish the potential diagnostic utility of sweat for monitoring kidney health. Below, we describe examples of advanced technologies for frequent, routine testing of biomarkers in sweat that can be performed without support facilities or specialized personnel.

**Creatinine detection.** Creatinine in sweat can be measured with sensors that use colorimetric reagents[35,45], surface-enhanced Raman scattering (SERS)[46] or electrochemistry[47,48]. For example, one microfluidic device collects sweat through a skin-interfaced inlet; it then passes through a series of microchannels and valves that route small volumes to a collection of chambers containing colorimetric reagents[35] (Fig. 2a). The sophisticated microfluidic design supports time-dynamic measurement of sweat metabolites, including creatinine, using the below reaction sequence:

$$\text{Creatinine} + H_2O \xrightarrow{\text{Creatininase}} \text{Creatine} \quad (1)$$

$$\text{Creatine} + H_2O \xrightarrow{\text{Creatinase}} \text{Urea} + \text{Sarcosine} \quad (2)$$

$$\text{Sarcosine} + H_2O + O_2 \xrightarrow{\text{Sarcosine oxidase}} \text{Formaldehyde} + \text{Glycine} + H_2O_2 \quad (3)$$

$$\text{4- Aminophenazone} + \text{Phenol derivative} + H_2O_2 \xrightarrow{\text{Peroxidase}} \text{Red benzoquinone imine dye} + H_2O \quad (4)$$

The device can measure creatinine over a linear dynamic range of 10–500 µM based on digital image analysis. Using this device, researchers have reported sweat creatinine concentrations of 10–15 µM for healthy individuals[35,45], which is consistent with other wearable electrochemical sensors[47,48] that report the range of 5–15 µM for healthy individuals (Table 1). Future studies involving patients with kidney disease are needed to determine whether measurements made with these wearable devices match previously reported sweat creatinine concentrations of 23–50 µM[43] (Table 1).

Other approaches operate based on the selective interaction of creatinine with metallo-organic frameworks (MOFs)[47,48]. These classes of biosensors exploit the chelating ability of creatinine with metallic centres through its five-membered ring, which contains two nitrogen atoms[49]. A 2021 study[47] reported a textile-based electrochemical sensor for the sensing of creatinine in sweat induced by exercise and heat stress. The devices used in that study wicked sweat through fabric threads to the sensing components. The sensor consisted of an electrochemical transducer attached to a nylon textile fibre coated with carbon black and a MOF recognition element consisting of cuprous nanoparticles encapsulated within a polyvinyl alcohol (PVA) hydrogel and a poly(3,4-ethylenedioxythiophene):polystyrene sulfonate (PEDOT:PSS) composite material. The cuprite ions form ionic cross-links between PVA and PEDOT:PSS and selectively chelate with creatinine over other interfering species such as glucose, uric acid, urea and NaCl in sweat, leading to amperometric responses[47]. The sensor has a linear range of 0.4–960 µM and a limit of detection of 0.06 µM. Studies in healthy humans that have used this approach to measure creatinine in sweat have reported concentrations comparable with those of other colorimetric studies (Table 1). Creatinine concentrations for healthy individuals increase to 40–60 µM[47] upon thermal stress and exercise, which overlaps with concentration ranges of 23–50 µM[43] recorded for patients with CKD (Table 1). These findings emphasize the need for strict sweat collection protocols to prevent false-positive results for kidney diagnostics.

**Urea detection.** The primary mode for detection of urea in sweat, as demonstrated using samples collected with skin-interfaced microfluidics[35,50] or textile fibres[51], involves the urease enzyme as follows[50–53]:

$$(NH_2)_2CO + 2H_2O \xrightarrow{\text{Urease}} CO_2 + H_2O + 2NH_3 \quad (5)$$

The resulting change in pH can be evaluated colorimetrically using standard pH papers[35], photonic interpenetrating polymer network films[50], phenol red solution[51] or polyaniline ink (PANI)[53].

Molecularly imprinted polymers (MIPs) represent a non-enzymatic approach to quantifying sweat urea[54] (Fig. 2b). Here, electropolymerization of 3,4-ethylenedioxythiophene around carbon and gold nanotubes in the presence of urea molecules, followed by elution of the embedded urea molecules, forms recognition sites in the MIP. The electron transfer resistance of a potassium ferricyanide probe with MIP-covered nanotubes changes upon the recognition of urea molecules. The sensor has a linear dynamic range of 1–100 mM and a

limit of detection of 0.1 mM, and in one study, successfully measured sweat urea concentrations of 14.4 mM, 12.5 mM and 30.3 mM in three individuals during exercise[54], where the first two values were within expected ranges for healthy individuals. The third measurement was high with unknown root cause, suggesting that further evaluation is required. Reported sweat urea concentration ranges are 2–15 mM[35] for healthy individuals and 22–33 mM[43] for patients with CKD, quantified by wearable colorimetric enzymatic sensors and standard optical spectrometric techniques, respectively (Table 1).

**Uric acid detection.** Differential pulse voltammetry is a convenient approach to detecting uric acid in sweat[42,55] (Fig. 2c). One study[42], which developed a laser-engraved wearable microfluidic device for collecting sweat samples generated by exercise, demonstrated time-sampled monitoring of uric acid levels for a period of 35 min. Sweat enters the device through the inlet holes and passes into microfluidic chambers that are interfaced with laser-engraved graphene sensors. Sweat uric acid and tyrosine concentrations are measured by detecting changes in current induced by application of linear ramp potential pulses, with detection limits of 0.74 µM and 3.6 µM, respectively[42]. In this system, a Bluetooth low-energy (BLE) system wirelessly transmits the resulting data to a user with a BLE-enabled device. Controlled human trials indicate strong correlations between uric acid concentrations in sweat and plasma and have revealed uric acid concentrations of 29–51 µM, 67–87 µM and 80–133 µM for healthy individuals, patients with gout and patients with hyperuricaemia, respectively[42], which are somewhat higher than previously reported concentrations of 10–35 µM[56]) and 20–60 µM[41] for healthy individuals and uraemic patients, respectively (Table 1). In those studies[41,56], sweat samples were collected using a plastic container and quantified using standard enzymatic well plate-based measurements. These discrepancies may result from differences in sweat-sampling methodology, variability in humans and/or quantification techniques. We expect future clinical wearable evaluations to provide valuable insights into the utility of sweat uric-acid concentrations for the monitoring of kidney health.

**Electrolyte detection.** Several studies have described wearable potentiometric sensors based on ion-selective electrodes for continuous quantification of sweat electrolytes such as $K^+$, $Na^+$, $Ca^{2+}$, $Mg^{2+}$ and $Fe^{2+}$ (refs. 23,57–61). In one study, a 3D-printed wearable device that resembled a watch measured sweat potassium concentrations during exercise[57]. Those sensors used poly(4-octylthiophene) as transducing layers, with screen-printed conductive carbon electrodes on polyethylene terephthalate (PET) sheets for electrical measurements. The reported responses were linear over a range of concentrations from 0.1 mM to 100 mM and with a detection limit of 0.1 mM[57]. The system, mounted on the upper arm, could track sweat electrolyte concentrations with BLE wireless data communication for analysis. The platform reported potassium concentrations of 1.65–7.25 mM in a healthy volunteer continuously during 90 min of exercise, covering physiologically relevant ranges for sweat potassium concentrations. Such wearable sensors will provide a useful platform for establishing correlations with disease status in patients with CKD.

## Interstitial fluids

ISF — the extracellular fluid located within the interstitial space around cells — provides oxygen and nutrients that are required for cellular metabolic processes[62]. ISF-based electrochemical sensors form a well-established basis for continuous glucose monitoring (CGM), which has been widely adopted in the form of small, wireless, skin-mounted devices[63]. Dermal ISF is rich in biomarkers, including proteins, metabolites, ions and RNA species, that correlate with those in blood[62–64]. Microneedles enable continuous electrochemical monitoring of various biomarkers[63] in ISF and are of interest because they penetrate only the dermis and therefore avoid damage to nerves or blood vessels. Alternative non-invasive methods of accessing ISF use reverse iontophoresis to extract ISF from the surface of the skin[64].

### Relevance of interstitial fluids for kidney disease

Clinical studies that have used microdialysis[65] or reverse iontophoresis[66,67] to access ISF have demonstrated the potential of these approaches to monitor biochemical markers of kidney health. One study used ISF microdialysate extracts collected every 15 min to provide insights into the kinetics of urea concentrations in 17 patients before, during and after haemodialysis[65]. Quantification using established enzymatic colorimetric urea tests demonstrated that ISF urea concentrations decrease during haemodialysis from 30 mM to 11.2 mM. This trend compares well with that of urea in plasma, where concentrations change from 29.8 mM to 11.4 mM. 4 h after cessation of dialysis, both ISF and plasma show increases in urea concentrations to 15.0 mM and 14.9 mM, respectively[65].

Reverse iontophoresis can also be used to extract ISF with relevant biomarkers for monitoring kidney health[68]. For example, reverse iontophoresis has been applied to the forearm of 5 healthy individuals and 18 patients with CKD to enable the analysis of urea in ISF using the colorimetric, diacetyl monoxime assay[67]. The findings demonstrated clear differences in ISF urea concentrations between healthy individuals and patients with CKD, with values of 22.3 and 50.7 µM, respectively. The sensitivity and specificity of this test in distinguishing patients with CKD from healthy individuals were 83.3% and 75%, respectively[40]. These data also showed that concentrations of urea in ISF correlate with those in plasma and support the use of ISF as a diagnostic fluid for kidney monitoring. Extension of this work to other biomarkers such as creatinine, uric acid and electrolytes through the use of other sensing modalities, along with alternative methods of accessing ISF, such as microneedles, provide additional options for the evaluation of ISF in the context of kidney health.

**Creatinine detection.** Microneedles and electrochemical sensors that use a cascade of enzymatic mechanisms have been used to measure creatinine concentrations in ISF[69] (Fig. 2d). Specifically, the microneedle body comprised a methacrylated hyaluronic acid, which forms a non-dissolvable, swellable polymeric matrix. The enzyme mixture, composed of creatininase, creatinase and sarcosine oxidase, modified screen-printed electrodes that interfaced with the microneedle arrays. Amperometric signals from $H_2O_2$ generated as a result of the enzymatic reaction with creatinine yielded a linear response across a range of concentrations from 50 µM to 550 µM with a limit of detection of 18 µM[69]. Application of this approach to a mouse model of CKD induced by intraperitoneal injections of aristolochic acid, demonstrated an increase in ISF creatinine concentration from 45 µM at day 0 to 85 µM at day 21 (ref. 69). Parallel measurements of serum creatinine concentrations revealed similar increases. These preclinical findings should motivate human trials to establish the utility of ISF creatinine assessment for monitoring kidney health.

**Urea detection.** Microneedle-based enzymatic sensors also enable real-time measurement of urea concentrations in ISF using potentiometric[69,70] methods. This approach uses the above-described platform for creatinine[69] but uses urease on the screen-printed electrodes, and yields a linear response for concentrations of 1–16 mM with a limit of detection of 0.49 mM[69]. Application of this method to mice with aristolochic acid-induced CKD demonstrated increasing urea concentrations from 3.8 mM (at day 0) to 7 mM (at day 21).

Other microneedle sensors contain an engineered microcavity on their tip to enable direct ISF sampling[70] (Fig. 2e). In one such example, the working electrode for potentiometric detection of urea consisted of a microneedle electrode array with a coating of Cr and Au. Subsequent coating of the microcavity surfaces with polyaniline boronic acid (PABA), urease enzyme and Nafion enabled recognition of urea molecules by the enzyme and sensing of the generated ammonia species by PABA. The sensor exhibits a linear dynamic range of 3 mM to 18 mM and a limit of detection of 0.9 mM. Evaluation of this sensor in mouse models indicated increasing potentiometric responses upon subcutaneous injection of different concentrations of urea for a duration of 10 min, designed to simulate increasing urea concentrations in ISF[70]. Extension of these animal model studies[69,70] to humans will provide further insights into the utility of these microneedle-based ISF urea sensing approaches for monitoring kidney disease.

**Uric acid detection.** Platforms[69] similar to those introduced above for the detection of creatinine and urea can also detect uric acid through the use of uricase functionalized working electrodes for amperometric detection. Sensors of this type exhibit a linear range of 31 μM to 1,000 μM with a limit of detection of 31 μM[69]. Application of this sensor in a mouse model of aristolochic acid-induced CKD demonstrated an increase in uric acid concentrations in ISF from 78 (day 0) to 257 μM (day 21)[69]. Extension of this work to healthy individuals and patients with CKD will shed more light on the use of ISF uric acid as a biomarker of kidney health.

**Electrolyte detection.** Microneedle-based sensor systems that use ion selective electrodes similar to those described above for sweat support real-time detection of different electrolytes in ISF, including $K^+$ (refs. 71–77), $Na^+$ (refs. 74–78), $Ca^{2+}$ (refs. 74,75,77), $Li^+$ (ref. 75) and $Cl^-$ (ref. 75). A 2022 study demonstrated the use of a potentiometric microneedle-based sensor patch for multiplexed monitoring of these five species of electrolytes[75] (Fig. 2f). The process for fabricating the sensing element used in that study involved coating an array of stainless steel microneedles with carbon ink and functionalizing them with multi-walled carbon nanotubes, followed by drop-casting of ion-selective membrane cocktails. The linear ranges for each sensor were 32–100 mM for $K^+$, 32–320 mM for $Na^+$, 10–100 mM for $Ca^{2+}$, 32–100 mM for $Li^+$ and 10–320 mM for, $Cl^-$. The limit of detection for each of these electrolytes was 15 μM, 18 μM, 3.9 μM, 12 μM and 8.4 μM, respectively. Electrolyte concentration measurements in rats indicated average ISF concentrations of 4.3 mM, 147 mM, 1.1 mM and 104.4 mM for $K^+$, $Na^+$, $Ca^{2+}$ and $Cl^-$, respectively[75]. Similar measurements in blood and serum samples demonstrated good agreement between ISF and blood, highlighting the on-body transdermal electrolyte measurement capability of the microneedle patch[75]. As for the above-described biomarkers, studies of patients with kidney disease are needed to establish the connection of electrolyte concentrations to disease conditions.

## Tears

Tears are produced by the lachrymal glands, and serve as a protective layer, lubricator and a cleansing agent on the surface of the eye[79]. Diagnostics based on tear biochemistry are of interest owing to the potential to form direct, non-invasive interfaces with this biofluid for continuous monitoring of biomarker concentrations. Tears contain ions, electrolytes, proteins, inflammatory cytokines and other species with great potential for health tracking[80,81]. Advances in microfluidics and engineering of biocompatible soft materials have led to the development of integrated contact lenses[82–93], eyeglasses[94,95] and tear patches[96] as wearable tear sensors. For example, smart contact lenses have been developed that use soft, breathable materials with biosensing capabilities for glucose, electrolytes and hormones[86,90–92]. Alternatives that use lab-on-eyeglasses and tear patches are also of interest because they do not require direct contact with the eye but instead collect stimulated tear flows under the eye[94,96].

### Relevance of tears for kidney disease

Exploratory clinical investigations based on conventional tear collection methods[81] have demonstrated the promise of tear biomarkers for renal diagnostics. A 1988 study used Schirmer sterile strips as a paper-based method for collecting tear samples to quantify concentrations of urea nitrogen and creatinine concentrations in tears from 30 healthy individuals and 10 patients with kidney failure[81]. Using established colorimetric assays based on urease[97] and the Jaffe method[98], concentrations of urea nitrogen were reported to be 3–7.5 mM and 6.8–27 mM for healthy individuals and patients with kidney failure, respectively, and concentrations of creatinine were 50–125 μM and 130–430 μM for healthy individuals and patients with kidney failure, respectively. Following dialysis, concentrations of urea nitrogen and creatinine in the tears of patients with kidney failure decreased to 3.8–16.0 mM and 50–280 μM, respectively. The data revealed a linear correlation between tears and blood for both of these chemical species[81], providing support for the notion that tear analytic platforms could provide a screening platform for kidney disease. As described below, further studies using state-of-the-art systems for the collection of pristine tear samples coupled with in situ biosensors could provide practical utility for the use of this biofluid.

**Creatinine detection.** A lab-on-eyeglass platform represents one interesting technology to quantify the concentration of creatinine in tears using a sensor based on selective interaction of creatinine with an MOF[95]. In one study[95] a source of camphor and menthol placed under the eye was used to stimulate the production of tears, and a nose pad structure that contained textile-based hybrid electrodes absorbed tears for amperometric detection of creatinine (Fig. 2g). The electrodes consisted of cotton fibre wrapped around flexible copper wires, coated with carbon black and cuprous nanoparticles. Subsequent electrochemical deposition of Cu(II)-benzene dicarboxylate (BDC) bound with graphene oxide-Cu(II) formed the MOF. Creatinine diffused into the porous architectures of the MOF and chelated with cuprous ions through irreversible catalytic binding. The sensor offered a linear range of 1.6–2,400 μM for the detection of creatinine, with a limit of detection of 0.8 μM, with minimal interferences from dopamine, glycine, urea and uric acid[95]. A light-emitting diode (LED) screen, integrated with the lab-on-eyeglass, displayed the results and a BLE module wirelessly transmitted data to an external device. Testing on healthy individuals revealed physiologically relevant concentrations of tear creatinine in real time for 8 min, ranging from 50 μM to

125 μM[95], and serum concentrations ranging from 50 μM to 130 μM[95], which agrees with previously reported tear creatinine concentrations of 50–125 μM[81] for healthy individuals and 130–430 μM[81] for patients with kidney disease (Table 1). Further studies are needed to determine the applicability of this platform for these patients and its utility in establishing a relationship between tear creatinine concentrations and kidney disease.

**Urea detection.** Urea can be analysed using the classic Jung method, which is based on the ability of a chromogenic reagent to form a coloured complex with urea[99]. Specifically, the reaction of urea, o-phthalaldehyde, and primaquine diphosphate produces yellow complexes. This type of colorimetric assay can be integrated into a contact lens, in which an integrated microfluidic system routes tears to reservoirs containing the assays (Fig. 2h). Quantification involves analysis of digital images captured using a smartphone[84]. The dynamic range of urea detection spans 0.078 mM to 2.5 mM, as evaluated with a model eye system with spiked artificial tear samples[84]. Additional work is needed to expand the range to that summarized for patients with kidney disease (Table 1).

**Uric acid detection.** Colorimetric enzymatic assays can also be integrated with sensing platforms on contact lenses for the measurement of uric acid (Fig. 2i). For example, one microfluidic device formed by multi-axis femtosecond laser ablation[87] to include flow valves, resistors, multi-inlet geometries and splitters uses a uricase enzyme-based sensing reaction to produce allantoin, hydrogen peroxide and $CO_2$, as summarized by the following chemical reaction:

$$\text{Uric acid} + H_2O + O_2 \xrightarrow{\text{Uricase}} \text{Allantoin} + CO_2 + H_2O_2 \quad (6)$$

This reaction is followed by the reaction of 4-amino antipyrine, *N*-ethyl-*N*-(2-hydroxy-3-sulfopropyl)-3,5-dimethoxyaniline and hydrogen peroxide in the presence of horseradish peroxidase to produce a blue dye, which is proportional to the reaction of uric acid. Optical evaluations enable assessments of urea concentrations with a linear range of 0.3–1.5 mM and with a sensitivity of 0.1 mM, based on tests with an artificial eye model[87]. This range matches expected requirements (Table 1), but human studies are required to validate this approach.

**Electrolyte detection.** Various fluorescence-based sensors can also be used on contact lenses to quantify tear electrolytes such as $K^+$ (refs. 91,100), $Na^+$ (refs. 85,89,91,100), $Mg^{2+}$ (refs. 91,100), $Cl^-$ (refs. 85,91), $Zn^{2+}$ (ref. 100) and $Ca^{2+}$ (refs. 91,100). One such device[100] contains laser-engraved microfluidic channels that collect and route tears to fluorescent probes. Tear electrolytes are selectively chelated by probes of varying sizes and chemistries, including crown ether derivatives for $Na^+$ and $K^+$, 1,2 bis(*o*-aminophenoxy) ethane-*N*,*N*,-*N*′,*N*′-tetraacetic acid for $Ca^{2+}$, 5-oxazolecarboxylic acid for $Mg^{2+}$ and *N*-(2-methoxyphenyl)iminodiacetate for $Zn^{2+}$ ions. Physiologically relevant detection ranges of 25–100 mM, 1–50 mM, 0.5–1.25 mM, 0.5–0.8 mM and 0.01–0.02 mM can be achieved for $Na^+$, $K^+$, $Ca^{2+}$, $Mg^{2+}$ and $Zn^{2+}$, respectively. A handheld fluorescence reader, with an integrated light source, battery power source and exchangeable bandpass filters, interfaces with a smartphone for quantification. Work in humans is necessary to validate these measurements and assess their value as a diagnostic tool in patients with kidney disease.

## Saliva

Saliva is produced by the salivary glands and is important for digestion[101]. As one of the most easily obtained biofluids, containing a rich range of electrolytes, hormones, metabolites, enzymes and proteins relevant to kidney biomarkers[101–103], saliva is an attractive target for biosensing. Current literature on saliva diagnostics mainly focuses on point-of-care systems[101] and on intraoral devices such as dental retainers[104] (Fig. 2j), mouthguards[105,106] (Fig. 2k) and pacifiers[107] (Fig. 2l).

### Relevance of saliva for kidney disease

Several clinical studies have examined the utility of saliva for monitoring kidney health[108–110]. Work from the past few years[108] has highlighted the potential of creatinine measurements in saliva to evaluate patients at various stages of CKD using an enzymatic colorimetric assay and saliva captured by spitting. Among 230 patients with CKD, saliva creatinine was 3–19 μM, 3–8 μM, 4–63 μM, 5–222 μM and 72–400 μM for patients with stage 1, 2, 3, 4 and 5 CKD, respectively[108]. The results of that study also established a strong correlation ($r = 0.82$) between serum and salivary creatinine concentrations. The sensitivity and specificity of salivary creatinine to distinguish patients with CKD from healthy individuals are 78.3% and 74%, respectively[108].

Another clinical study assessed creatinine, uric acid and potassium in 15 healthy volunteers and 42 patients with CKD[109]. Saliva samples obtained with a cotton swab and rapid centrifugation were analysed using commercially available kits to enzymatically quantify the concentrations of creatinine and uric acid. Potassium concentrations were assessed by ion-selective potentiometry. Concentrations of these biomarkers in saliva were 10–20 μM, 60–450 μM and 18–60 μM for creatinine, uric acid and potassium, respectively, in the control group. For patients with CKD, salivary concentrations of creatinine, uric acid and potassium were 15–145 μM, 60–500 μM and 15–70 μM, respectively. Significantly different salivary creatinine concentrations in the control and patient groups support the use of this species as a diagnostic biomarker. Concentrations of these biomarkers correlate with those in plasma. Furthermore, concentrations measured post-dialysis mirror those in plasma, supporting the use of saliva as a diagnostic fluid[109]. Clinical studies of salivary biomarkers provide motivation for the development of wearable analytic platforms that use saliva for monitoring of kidney health.

**Uric acid detection.** One study reported the development of a sensor in the form of a mouthguard that included an enzymatic electrochemical sensor for the real-time quantification of salivary uric acid[106] (Fig. 2k). The sensor uses uricase as the recognition element and a Prussian blue carbon electrode as the transducer, and detects salivary uric acid with a linear range of 50 μM to 1,000 μM and stability of up to 4 h (ref. 106). The amperometric sensor is coupled with miniaturized instrumentation electronics that include a potentiostat, microcontroller and a BLE wireless communication system for real-time data acquisition and communication. Benchtop testing based on saliva samples from a healthy volunteer and a patient with hyperuricaemia reported uric acid levels of 178.5 μM and 822.6 μM, respectively[106]. Salivary concentrations of uric acid in the patient with hyperuricaemia were also higher than those reported from benchtop validation studies in healthy controls[109] (Table 1). In addition, salivary uric acid concentrations in the patient decreased to 300 μM following a 5-day treatment course of allopurinol, a drug that lowers high uric acid concentrations in blood.

**Electrolyte detection.** A 2022 study reported the development of a bioelectronic pacifier device that includes ion-selective electrodes for the continuous monitoring of sodium and potassium concentrations in the saliva of neonates[107]. The device captures saliva samples through an inlet hole located at the tip of the pacifier that leads to a microfluidic channel to the ion sensors. The device includes a flexible circuit with BLE wireless communication and a rechargeable battery, and sensor stability has been demonstrated over 10 h. The ion sensor detects salivary sodium and potassium concentrations with a linear range of 1–100 mM[107]. Studies in the neonatal intensive care unit show that the sensor can detect sodium concentrations of 6–9 mM[107] and potassium concentrations of 4–5 mM[107] continuously in real time for 1 h. These results are physiologically relevant considering previously reported values of 6–217 mM[111,112] and 3–18 mM[112] for salivary sodium and potassium concentrations, respectively (Table 1).

## Challenges and future directions

### Sensor performance

Concentrations of kidney-related biomarkers in peripheral biofluids are often lower than those in serum[27] (Table 2). Hence, efforts to develop practical technologies must consider the performance parameters that are physiologically relevant for the respective biofluids[27] and place the context of use for the various technologies into a laboratory medicine quality and consistency framework. As peripheral biofluids contain unique mixtures of biochemicals[33], transduction or detection mechanisms may be adversely affected by biofouling (with proteins, mucin, peptides or enzymes), interference from redox-active molecules (such as pH, uric acid, ascorbic acid or acetaminophen) and other species (such as salt and bilirubin). Contamination from debris, blood, sebum and other species that are often present in biofluids can also hinder biomarker measurements. Improvements in device and sensor architectures to reduce these interferences, along with innovative contaminant-free biofluid collection strategies, are critical for reliable biosensor performance.

Another difficulty associated with the use of wearable devices for clinically relevant assessments compared with the evaluation of samples collected and separately evaluated in laboratory environments is that stable, accurate operation must occur under dynamic and poorly controlled conditions. Variations in secretion rates and volumes, skin temperature, body orientation and motion, together with variations in environmental conditions such as lighting, humidity and ambient temperature, can lead to inaccuracies[33]. Advances in biosensing assays, engineering designs and calibration techniques provide routes to addressing these issues.

### Biocompatibility

Wearable devices must, of course, be biocompatible, safe and comfortable[83,87]. These requirements can be challenging for contact lens platforms because the human eye is highly sensitive to foreign objects[113]. However, even the intra-oral operating environment in the context of saliva sensors imposes some restrictions, as the device and sensing materials may readily dissolve in saliva or be swallowed[101,103]. For minimally invasive sensors such as microneedles that penetrate the skin, localized irritation, infection, inflammation and heating can be problematic[33,62,63]. By contrast, skin-interfaced microfluidic devices for sweat analytics suffer less from these limitations, as evident from the many human trials reported in the literature. Continued development of non-invasive, non-toxic and fully miniaturized sample collection techniques, biosensing assays and electronic components are expected to provide more comfortable, safe and painless experiences for users in the future[79,83].

### Clinical studies and correlations with blood

Most studies of wearable devices for the evaluation of kidney biomarkers have involved proof-of-concept demonstrations on simple animal models or a small number of healthy individuals[27]. In addition, human research using biofluids sampled from sensitive sites, such as the eye, the interstitial space and the mouth, is particularly limited. In these cases, validation studies often involve artificial biofluids in benchtop settings or animal models, which have some, albeit limited, relevance to human tears, ISF and saliva chemistry. Future work is therefore needed to determine the biocompatibility, wearability and accuracy of these methods in scaled human studies.

Many factors affect the concentrations of biomarkers in biofluids, such as the use of stimulation methods, the method used to partition the biomarker from blood, and the metabolic action of the secreting glands[34,79]. In the case of sweat, several stimulation methodologies are available[114] including sauna, exercise and pharmacological approaches. Each method produces different rates of sweating, biomarker concentrations and pH. Partitioning of a biomarker in these and other cases depends on multiple factors, including the time elapsed since stimulation as well as the secretion rate and volume of the biofluid. Establishing correlations of biomarker concentrations to blood in a manner that accounts for these various factors is important for clinical utility in renal monitoring[36].

### Towards continuous monitoring of biomarkers

Currently, most wearable biosensors provide a single-point read-out of biomarker concentrations[35,54,69,84,87,115]. Although these devices have potential as convenient point-of-care tools for routine monitoring of key biomarker concentrations, biosensors that can take continuous measurements have even greater value[42,70,75,95,104,106,107]. Typical methodologies for wearable continuous biosensing involve the use of enzymes or electrochemical sensors to detect metabolites[42,70,95,106] or ion-selective electrodes to detect electrolytes[75,104,107]. Alternative schemes such as those that use active reset aptamer-based sensors[116], antibody or aptamer-based molecular switches[117,118] and microfluidic real-time ELISAs[119] are emerging as potential candidates for continuous sensing of proteins or hormones. Several challenges exist for these and related technologies, such as biofouling, interference from redox-active molecules, complicated sample preparation methodologies, the need for precise tuning of the affinity of biorecognition elements and the need for continuous biofluid sampling. However, strategies that overcome these challenges will have broad value in monitoring not only kidney health but many other conditions.

## Implantable devices

Although wearable sensors enable non-invasive and often facile data collection, some renal complications[120–122] such as transplant rejection and viral infections can result in highly localized symptoms within the kidney. In these cases, biomarkers of kidney dysfunction may not be present in sufficient concentrations in peripheral biofluids and changes in the physical properties of the kidney (such as temperature, morphology or stiffness) may not manifest as gross external or systemic symptoms. In these instances, local measurements of the biophysical properties of the kidney through the use of implanted devices may offer enhanced sensitivity in detecting early disease onset.

Most implantable devices for monitoring the local properties of the kidney consist of a probe that contains the core sensing component (for example, LEDs or photodiodes for optical measurements and temperature sensors or heaters for thermal measurements) connected to an electronics module that includes circuitry for signal transduction, with either wireless data communication or wired data acquisition electronics (Table 3, Fig. 1). The size of the probe and electronics module are limited by manufacturing technologies and the power source (for example, the battery), respectively. Device-operating lifetimes for battery-powered devices are governed by the power consumption and sampling frequency of the measurement; battery-free power transfer approaches (such as ultrasound[123] or magnetic inductive coupling[124]) circumvent the limitations of a battery but require an external source to power the device. These devices can be secured to the kidney through the use of sutures, bioresorbable barbs and/or van der Waals adhesion forces and contain biocompatible encapsulation materials[125–127] including parylene-C, polyimide and silicones. Specific examples of implantable technologies that can be used to monitor kidney perfusion during surgery, AKI, kidney transplant rejection and kidney cryopreservation are discussed below.

### Local tissue oxygenation as a measure of perfusion

Regional measurements of tissue oxygenation ($StO_2$) can offer insights into vascular health[128,129]. Such data can help to prevent surgical complications, such as renal artery or vein thrombosis (typically <1% incidence) and renal artery stenosis (1–10% incidence), that can occur during transplantation. These and other types of complications can result in graft loss even up to a few years post-operation[130]. In similar contexts, ischaemia–reperfusion injury (IRI) can cause acute tubular necrosis and delayed graft function upon reoxygenation of the tissue[131].

A 2022 study reported the development of a wireless, implantable optoelectronic device for continuous monitoring of $StO_2$ in the kidney[128]. In addition to local measurements of $StO_2$, the device could detect the pulsatile component of blood flow (heart rate) and respiration rate. The device comprises a flexible optical probe for near-infrared spectroscopy (NIRS) measurements, using two microscale LEDs (μ-LEDs) with peak emission wavelengths of $\lambda_1 = 660$ nm (red) and $\lambda_2 = 850$ nm (near-infrared), respectively, and two microscale photodiodes (μ-PDs) (Fig. 3a). The probe connects to a flexible battery-powered module with electronics for sensing and wireless data transfer to any 'smart' portable device via Bluetooth (Fig. 3).

NIRS relies on the absorption of red light by deoxyhaemoglobin (Hb) and that of near-infrared light by oxyhaemoglobin ($HbO_2$). The two μ-PDs, separated laterally by 4 mm and 7 mm from the LEDs, enable spatial probing of tissue volumes of approximately 95.3 and 178 $mm^3$ for the red and near-infrared wavelengths, respectively. Increasing the distance between the μ-LED and μ-PD increases these volumes. The multi-wavelength and multi-detector design enables calculations of $StO_2$ with a single external calibration:

$$\begin{bmatrix} kC_{Hb} \\ kC_{HbO_2} \end{bmatrix} = \frac{1}{\ln(10)} \begin{bmatrix} \varepsilon_{Hb,\lambda_1} & \varepsilon_{HbO_2,\lambda_1} \\ \varepsilon_{Hb,\lambda_2} & \varepsilon_{HbO_2,\lambda_2} \end{bmatrix}^{-1} \begin{bmatrix} k\mu_{a,\lambda_1} \\ k\mu_{a,\lambda_2} \end{bmatrix} \quad (7)$$

$$StO_2 = \frac{C_{HbO_2}}{C_{HbO_2} + C_{Hb}} \quad (8)$$

where $\varepsilon_{Hb}$ or $HbO_2$, $\lambda_1$ or $\lambda_2$ is the specific molar extinction coefficient for Hb or $HbO_2$ at $\lambda_1$ or $\lambda_2$, $\mu_a$ is the tissue absorption coefficient and $k$ is an unknown constant that is cancelled out during the calculation of $StO_2$. By contrast, a single LED and PD probe architecture requires baseline calibration with the initial $StO_2$ at $t = 0$ and knowledge of total haemoglobin concentration ($C_{Hb,t}$):

$$StO_2(t) = \frac{C_{Hb,t} \times StO_2(t=0) + \Delta C_{HbO_2}(t)}{C_{Hb,t} \times StO_2(t=0) + \Delta C_{HbO_2}(t) + C_{Hb,t} \times (1 - StO_2(t=0)) + \Delta C_{Hb}(t)} . \quad (9)$$

A bioresorbable barbed structure that surrounds the probe, formed with an FDA-approved bioresorbable polymer (PLGA), supports safe removal of the device after the intended use period (~1 month). Probes with barbs exhibit a ~40% reduction in translation distance within the tissue compared with those without barbs over a 4-week period, as confirmed through X-ray CT in rat models. Dissolution of the barbs occurs within 10–14 days after implantation, consistent with a reduction in pulling force to ~0 N, thereby facilitating device removal without damage to adjacent tissues. Rat models implanted with barbed devices exhibited no difference in toxicity indices compared with control animals with sham surgeries.

The utility of the device has been demonstrated in a porcine kidney model of IRI (Fig. 3c). Fast Fourier transformations of the $StO_2$ data revealed that the heart rate (1.7–2.5 Hz) and respiratory (~0.3 Hz) signals disappeared during vessel occlusion, serving as a binary indication of the loss of blood flow (Fig. 3d). Although this in vivo work was conducted in anesthetized pigs, the use of such devices in ambulatory settings must address uncertainties in the measured $StO_2$ that result from motion (for example, through algorithms[132–134] or the use of additional electromechanical sensors such as accelerometers, gyroscopes[135,136], or pressure[137] or strain sensors[24,138]). Challenges in monitoring $StO_2$ across chronic timescales include the need to eliminate drifts in the signals[129] resulting from changes in the optical or physical properties of the surrounding tissue (for example, fibrotic tissue or other foreign body responses, thickening of the renal capsule) and the need to engineer the dissolution time[139,140] of the barbs to reach timescales (~few years) required for monitoring of post-surgical vascular health.

### Thermal sensing of microvascular flow on the near-surface of kidney tissue

Analogous to optoelectronic probes[128], thermal flow sensing probes have been developed to assess microcirculatory flow on the surface of the kidney as an indication of perfusion[141]. The dimensions of the probe are comparable with a 12-gauge biopsy needle (~2 mm in diameter). The probe itself contains a surface mount (SMT) heater, surrounded by a circular thin-film heat spreader on the back side of a polyimide flexible printed circuit board (fPCB), and four SMT thermistors spaced at different lateral distances from the heater (#1, directly underneath the heater to #4, ~8 mm from the heater), on the front side of the fPCB (Fig. 3e). Measurements from thermistor #4 are relatively insensitive to the heater temperature and enable measurements of changes in ambient temperature. Subtracting changes in temperature captured by thermistor #4 from those obtained from thermistors #1–3 minimizes the effects of ambient temperature. Similar to the above-described optoelectronic probe[128], the thermal probe contains bioresorbable barbs (Fig. 3f) for anchoring underneath the renal capsule; a separate electronics module contains sensing and BLE communication circuitry.

The above-described device records the temperature change of the surface of the kidney from thermistors #1–4 as a function of time while the heater locally warms the tissue to no more than 4 °C of the

**Table 3 | Implantable devices for monitoring of kidney health**

| Measurement | Form factor | Size[a] | Electronics size limitation | Minimum probe size | Maximum probe size | Device lifetime (limitation) | Surgical anchor to kidney | Encapsulation materials | Application | Ref. |
|---|---|---|---|---|---|---|---|---|---|---|
| Temperature, thermal conductivity | Thin, stretchable thermal probe connected to electronics module | ~0.7×0.3×0.02 $cm^3$ probe<br>~1.6×1.1×0.5 $cm^3$ electronics | Battery, circuit components (BLE antenna) | Limited by practical lithographic patterning process to minimum areas of ~10s of micrometres | Tunable to several centimetres by lithographic patterning/ substrate size | 2.5 months, limited by power consumption (battery capacity or mechanical and chemical reliability) | Sutures to renal capsule | Silicone, polyimide, polyolefin | Kidney transplant rejection<br>AKI | 142 |
| Temperature, perfusion | Thin, flexible probe containing heater/temperature sensor array connected to electronics module | ~2×0.02×0.01 $cm^3$ probe<br>~5×4 cm electronics, thickness not reported | Battery, circuit components (BLE antenna) | Limited by size of surface mount electronic components and PCB manufacturing processes to ~ 1×2 $mm^2$ areas (3 SMD resistors) | Tunable to several centimetres by component arraying or use of large SMD components | Not reported; limited by power consumption (battery capacity or mechanical and chemical reliability) | Bioresorbable barbs into cortex | Polyimide, silicone | Kidney transplant rejection<br>AKI | 141 |
| $StO_2$ | Thin, flexible probe containing LED/PD array connected to electronics module | ~1.3 x 0.06×0.04 $cm^3$ probe<br>~1×2 $cm^2$ electronics, thickness not reported | Battery, circuit components (BLE antenna) | Limited by size of surface mount electronic components, PCB manufacturing process to ~ 640×600 $\mu m^2$ areas (1 LED, 1 PD) | Tunable to several centimetres by component arraying or use of large SMD components | Not reported; limited by power consumption (battery capacity or mechanical and chemical reliability) | Bioresorbable barbs into cortex | Parylene-C, silicone | AKI | 128 |
| Perfusion, temperature, heat flux, thermal contact resistance | Thin-film probe containing heat flux sensor, heating element and temperature sensor, which are wired to an external electronic data acquisition system | 19.79 $cm^2$ circular area × 0.041 cm thickness | N/A | Limited by patterning/ manufacturing process[b] | Tunable by patterning process and substrate size | N/A, mechanical reliability | Van der Waals adhesion | Mylar, thermally activated epoxy | Kidney cryopreservation | 155 |

AKI, acute kidney injury; BLE, Bluetooth low-energy; LED, light-emitting diode; NA, not applicable; PCB, printed circuit board; PD, photodiode; SMD, surface mount device. [a]Sizes reported as length × width × height unless noted otherwise. [b]Exact patterning process unknown — proprietary information of commercial vendor.

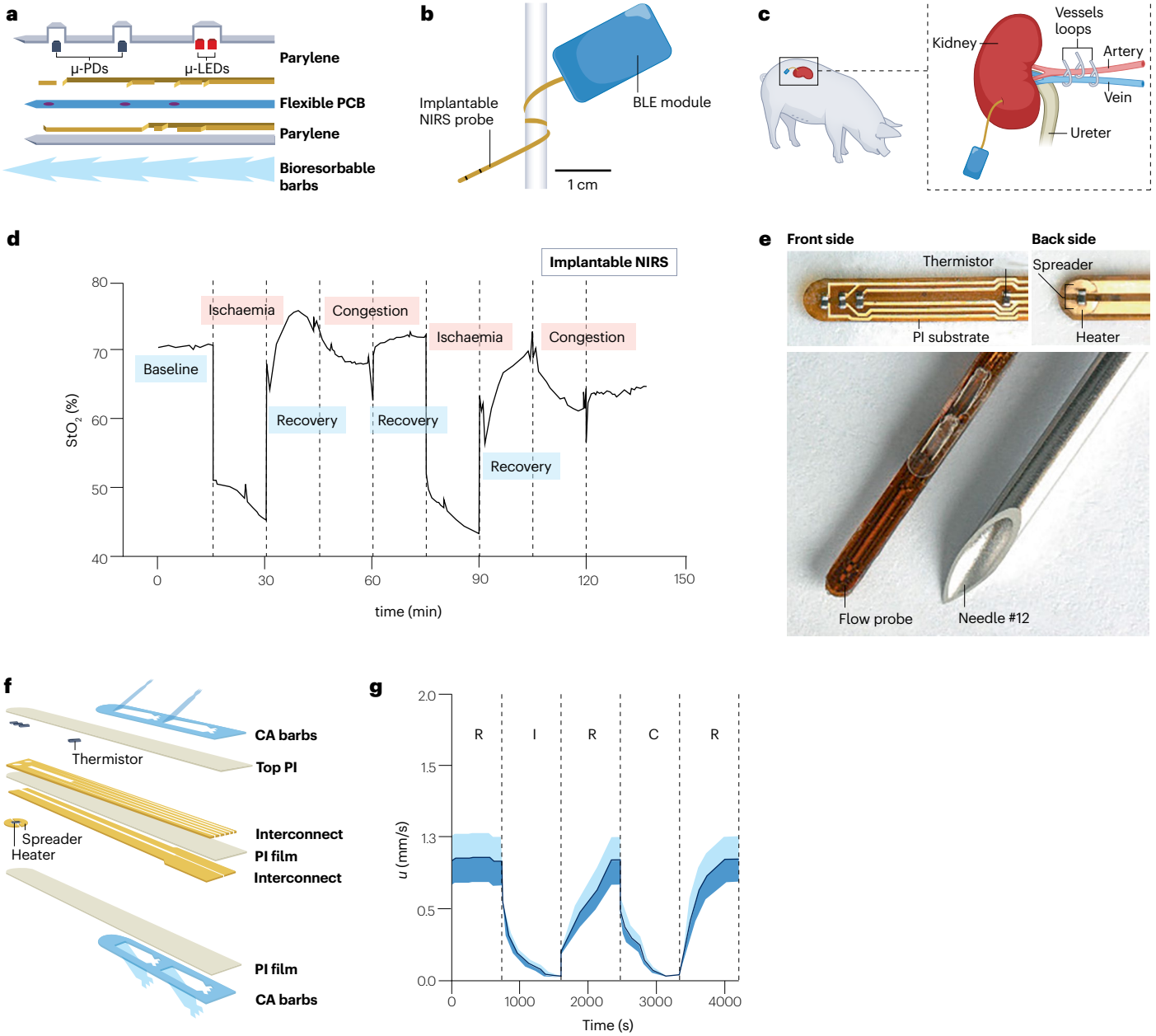


**Fig. 3 | Implantable sensors for monitoring tissue perfusion. a**, Schematic of the constituent layers of a near-infrared spectroscopy (NIRS) probe. The probe consists of a pair of μ-LEDs (light-emitting diodes) and μ-PDs (photodiodes) electrically connected to a flexible printed circuit board (PCB). The sensing structure is coated on all sides by a biocompatible, insulating polymer (Parylene-C). A bioresorbable barb structure made of PLGA is attached to the device on the opposite side of the optical sensing components. **b**, Optical image of a wireless, optical sensing device, consisting of an NIRS probe (single LED and photodiode array) and a Bluetooth low-energy (BLE) module for data transfer, which also contains sensing electronics. **c**, Schematic of the porcine model of ischaemia–reperfusion injury depicting the location of the NIRS device on the kidney. The NIRS device is implanted underneath the renal capsule. **d**, In vivo measurements of tissue oxygenation saturation ($StO_2$) on a porcine kidney during periods of ischaemia and reperfusion. **e**, Optical image of a thermal flow probe for measurements of local tissue perfusion (flow rate) in comparison with a #12 needle. The thermal flow probe consists of a resistive heater soldered to the back side of a flexible printed circuit board (fPCB) and four thermistors soldered to the front side of the fPCB, one directly above the heater, separated by the core dielectric layer of the fPCB, polyimide (PI), and the other three thermistors at different distances away from the heater. **f**, Schematic of the layers of the thermal flow probe. The probe consists of heaters and thermistors electrically connected to a fPCB, coated by insulating PI and bioresorbable barbs made of cellulose acetate (CA) on the top and bottom. **g**, In vivo measurements of renal cortical flow rate in a porcine model of ischaemia–reperfusion injury to the kidney. 'R' denotes recovery, 'I' denotes ischaemia and 'C' denotes congestion. Parts **a**–**d** are adapted from ref. 130, CC BY 4.0 (https://creativecommons.org/licenses/by/4.0/). Parts **e**–**g** are adapted with permission from ref. 141, Elsevier.

initial temperature, consistent with FDA guidelines on the safety of clinical devices. The temperature change measured by each thermistor relates to the flow rate $u$ according to

$$\Delta T \approx \frac{qR/k}{1+0.76s\sqrt{\frac{uR}{\alpha_{\text{fluid}}}}} F\left(\frac{r}{R}\right) \quad (10)$$

where $q$ is the thermal power per unit area delivered to the tissue by a heater of known radius $R$, $r$ is the separation between the thermistor and the centre of the heater, $k$ is the effective thermal conductivity of the tissue, $s$ is the volume fraction of blood in the tissue, $\alpha_{\text{fluid}}$ is the thermal diffusivity of the fluid, and $F\left(\frac{r}{R}\right)$ is a non-linear function describing the geometry of the heater and sensor. Values of $q$, $R$ and $r$ depend on the device geometry; $s$, $k$ and $\alpha_{\text{fluid}}$ are from the literature or measured experimentally; and $\Delta T$ is measured by the device. Thus, $u$ is the only unknown. The perfusion $w$ can be obtained from the value of $u$, following

$$w = \frac{uA_{\text{vessels}}}{V} \quad (11)$$

where $A_{\text{vessels}}$ represents the effective total cross-sectional area of the microvascular blood vessels and $V$ is the total tissue volume. Validation of the analytical model (Eqs. 10,11) was achieved using a 3D-printed model of microvascular tissue comprising ~100-μm-diameter channels formed in a poly(dimethylsiloxane) (PDMS) matrix. A syringe pump introduced a flow of water into the channels at known flow rates; the analytical model showed good (~1:1) agreement with an in vitro model for microvascular flow, hence validating the device design and analysis approach.

In vivo experiments in a porcine kidney determined a blood flow rate, $u$ value of 0.9 ± 0.2 mm/s during reperfusion. The corresponding value of perfusion $w$ (35 ± 11 ml/100 ml min) is consistent with those of transplanted kidneys. During ischaemia and congestion, $u$ values of 0.03 ± 0.01 and 0.04 ± 0.01 mm/s, respectively, indicate a near absence of perfusion (Fig. 3). Although this in vivo demonstration highlights the potential value of monitoring perfusion during solid organ transplantation, further work must consider the possibility of time-dependent variations in $s$, $k_{\text{tissue}}$ and $\alpha_{\text{blood}}$ in the tissue. Integration with other sensors such as those for $StO_2$ may mitigate uncertainties in $u$ and $w$ values by offering real-time, empirical estimates of the volume fraction of blood in tissue, $s$.

### Temperature

In addition to thermal measurements of perfusion, we have reported[142] the development of a fully implantable bioelectronic system that measures local kidney temperature for applications in kidney transplant rejection (Fig. 4a). The device contains a small (0.3 × 0.7 $mm^2$), ultrathin (0.22 mm) stretchable thermal probe (up to an elastic limit of ~20%) comprising a thin film of gold (100 nm), insulated by a layer of polyimide (10 μm) and silicone (100 μm) on either side (Fig. 4b). Similarly to the above-described optoelectronic and thermal probes[128,141], this probe connects to a battery-powered electronics module that contains circuitry for sensing and communication via BLE.

The device switches between two modes of operation. The temperature mode relies on a linear change in the resistance of the gold filamentary sensor[143] with temperature, whereas the thermal conductivity mode relies on the transient plane source method, where current (~1.7 mA) passing through the sensor for ~22 s results in local heating (by no more than 2 °C above the initial temperature of the tissue). The change in temperature at the surface of the kidney ($\Delta T$) during this heating period relates to $k_{\text{kidney}}$ using the relationship

$$\frac{\Delta T k_{\text{kidney}}}{2qR} = f\left(\frac{\alpha t}{R^2}\right) \quad (12)$$

where $R$ is the radius of the sensor, $t$ is the heating time, $\alpha$ is the tissue thermal diffusivity and $f$ is a non-linear function given by

$$f\left(\frac{\alpha t}{R^2}\right) = \frac{2qR}{k}\int_0^\infty \left\{[J_1(x)]^2 \text{erf}\left(x\sqrt{\frac{\alpha t}{R^2}}\right)\right\}\frac{\mathrm{d}x}{x^2} \quad (13)$$

where $J_1(x)$ is the first-order Bessel function of the first kind and erf($x$) is the error function.

Equation 12 contains an additional factor of 2 to account for the surrounding tissue medium inside the body, in contrast to that used for the above-described thermal sensor[144] (Eq. 10), where the device is exposed to air on one side ($k_{\text{air}} \approx 0.02$ W/m-K). Local kidney temperature ($T_{\text{kidney}}$) is a metric for tissue inflammatory response, whereas thermal conductivity of the kidney ($k_{\text{kidney}}$) serves as a measure of perfusion. In this work, we demonstrated that $k_{\text{kidney}}$ for a rat with a single kidney is ~2 × that with both kidneys ($k_{\text{kidney}}$ = 0.33 W/m-K), as might be expected.

Isogeneic and allogeneic rat models of kidney transplantation with different major histocompatibility complexes result in graft acceptance or acute rejection, respectively (Fig. 4c). Using our bioelectronic sensor, we reported a surgical recovery period over ~2 days, followed by the emergence of a normal circadian rhythm (frequency $f$ = 1 per day) in $T_{\text{kidney}}$ thereafter for isogeneic transplants, signifying a normal, healthy response, similar to that of control animals without transplantation. However, in allogeneic transplants we observed a 'bump' feature in $T_{\text{kidney}}$ of magnitude ~0.6 °C, which started ~3 days after transplantation. At the onset of this bump, values of serum BUN and creatinine were within the normal range. During days 5–6, the temperature of allogeneic kidneys fell steeply by −0.5 °C per hour to ~30 – 32 °C, concurrent with a marked change in animal behaviour and motion and elevated values of BUN and creatinine. The histological morphology of the kidney indicated rejection both at the onset of the bump feature on day 3 and the during the sharp decline on days 5–6, indicating the ability of temperature to identify rejection in advance of changes in BUN and creatinine. Complementary experiments involving the continuous administration of immunosuppressive therapy to recipient rats with allogeneic transplants demonstrated a similar but smaller (~0.15 °C) 'bump' feature in $T_{\text{kidney}}$, along with ultradian rhythms at frequencies $f$ = 2 and 3 per day (Fig. 4d). These ultradian rhythms are higher frequency rhythms than the circadian rhythm, occurring twice and three times per day, respectively. In our study, these rhythms could be used to detect kidney transplant rejection with 100% accuracy and with a true-positive rate of 100%. By contrast, the corresponding assessments of serum creatinine had an accuracy of only 54% and a true-positive rate of 17%. Although the underlying cause of these ultradian rhythms is not well known, related rhythms appear in cases of inflammatory bowel disease (IBD)[145], in which variations in intestinal temperature correlate with serum concentrations of inflammatory cytokines[145]. Of note, T cell activity is responsible for both the progression of IBD[146] and acute kidney graft rejection[122].

By comparison with $T_{\text{kidney}}$, measurements of $k_{\text{kidney}}$ do not display clear indications of graft rejection. The kidney's glomerular filtration rate may overshadow a change in perfusion from the rejection response. Further work is needed to elucidate the changes that occur

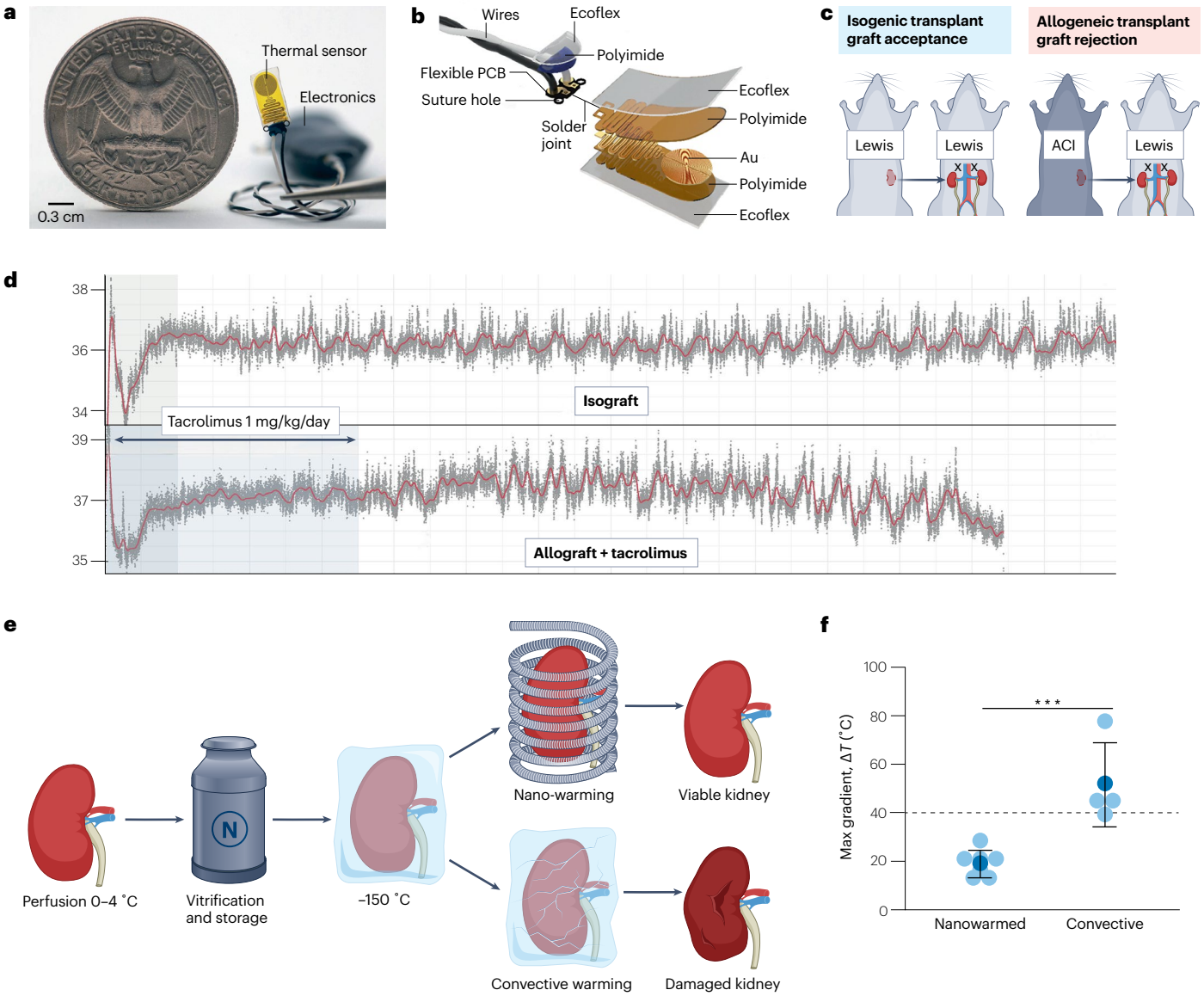


**Fig. 4 | Implantable temperature sensors for monitoring kidney transplant health. a**, Optical image of a fully implantable, wireless system comprising a multimodal, stretchable thermal probe connected to an electronics module. **b**, Schematic of the layers of the thermal probe. A 100-nm-thick layer of gold (Au) forms the core sensing layer and is coated on either side by a 10-μm layer of polyimide, which chemically protects the sensing layer from fluids and mechanically isolates it from mechanical motion. The entire sensing structure is coated in a 100-μm-thick layer of a low-modulus formulation of silicone, 'Ecoflex.' Gold pads on the sensor are connected to a pair of multi-stranded wires by way of a flexible printed circuit board (PCB) and solder joints. The solder joint is electrically insulated with polyimide and coated in the same Ecoflex material, which serves as a soft interface to the tissue. **c**, Schematic of the rat model of kidney transplantation for isogeneic (Lewis donor and recipient) and allogeneic (ACI donor and Lewis recipient) transplants. The native kidneys, which have been removed, are indicated by 'x'. **d**, Temperature of the kidney as a function of time for an isogeneic transplant (top) and allogeneic transplant treated with FK506 (tacrolimus) 1 mg/kg for 7 days post-transplantation (bottom). 15, xxx; F1, xxx. **e**, Schematic of kidney freeze–thaw cycles via nano-warming (inductive) and traditional convective heating approaches. **f**, Maximum gradient in temperature across the kidney during nano-warming and convective heating approaches. ***$P < 0.001$; two-tailed, unpaired *t*-test; error bars, s.e.m. Cor, cortex; hil, hilum; med, medullar; out, outside the kidney. Parts **a**–**d** are adapted with permission from ref. 142, AAAS. Parts **e** and **f** are adapted from ref. 156, CC BY 4.0 (https://creativecommons.org/licenses/by/4.0/).

in renal blood flow in various locations of the kidney during rejection. Promising areas for additional study include the application of similar sensing approaches for other types of rejection, including chronic rejection[147] and antibody-mediated rejection[148], and for other types of organ transplants, such as liver[149] and lung[150]. Moreover, the ultradian rhythms and 'bump' feature observed here may not be unique to renal graft rejection; future work should explore temperature variations related to other renal, adjacent-organ, or systemic conditions.

Temperature and thermal conductivity measurements on the kidney surface also have utility for monitoring the re-warming and perfusion of cryopreserved organs[151–155] — a critical procedure that is performed prior to transplantation. Two studies have reported a vitrification and 'nano-warming' technique, where alternating magnetic fields induce heating in low-toxicity cryoprotective agents (CPA) and silica/polyethylene glycol-coated iron oxide nanoparticles within the organ. This approach enables uniform, rapid warming of the kidney prior to transplantation[151,154] (Fig. 4e). Placement of fibre optic temperature probes in the hilum, medulla, cortex and outside the kidney to record temperature distributions demonstrated that nano-warmed kidneys yielded much smaller temperature gradients than those induced by convective warming in a water bath (<25 °C and >40 °C, respectively) (Fig. 4f). Such uniformity is important to prevent cracking of the tissue from thermal stress. A warming rate that is too slow could also result in ice crystallization, further highlighting the importance of temperature monitoring during the freeze–thaw process.

Rats that received nano-warmed kidneys showed statistically significant differences in levels of serum creatinine and other biomarkers (potassium, pH, $HCO_3$, $pCO_2$ and lactate) ~10–15 days post-transplantation compared with those of rats transplanted with fresh, control transplants. At day 30, serum and urine biomarkers exhibited normal values; renal histology was similar between nano-warmed and fresh kidneys. These findings suggest that nano-warming could provide a potential solution for donor kidney loss in organ banking, with opportunities for continued study with large animals and assessment of long-term graft survival.

## Challenges and future opportunities

**Sampling error.** Sensors, like biopsies, have the advantage of detecting changes occurring at specific locations on the kidney[156]. However, they both suffer from sampling error when the diseased tissue is distant from the measurement site. To reduce this error, a device with multiple probes or larger sensing areas is needed to capture adequately large sample areas.

**Sensitivity and specificity.** For a particular sensing approach, high specificity and high sensitivity are both necessary for reliable detection of disease onset[157]. Confounding factors can impact specificity; for instance, in addition to AKI or kidney transplant rejection, diet can alter serum creatinine levels[158]. A device that is engineered with high specificity for only a particular disease may fail to identify the onset of other conditions that require medical attention. Because any warning sign can prompt further clinical evaluation to enable appropriate intervention, measurement sensitivity is the most significant enabler of early disease detection. Increasing sensor resolution and engineering device designs that enable signal collection without influence from unrelated factors (for example, motion artefacts and environmental conditions) may improve measurement sensitivity. Use of a combination of biomarkers may help to improve the specificity of particular sensors[122].

**Foreign body reactions.** Evaluating foreign body reactions (FBRs) to devices implanted in large animals for varying durations would help to determine the feasibility of implantable devices for the monitoring of acute and chronic conditions. FBRs can involve the formation of foreign body giant cells, which attempt to break down the foreign material; the formation of fibrotic capsules that isolate the device from the surrounding tissue; and chronic inflammation[159,160]. These adverse reactions can impede device functionality and/or cause damage to surrounding tissues and pain or discomfort to the patient. In one study[161], FBRs affected 43 of 292 (~15%) of patients who had received an implanted pacemaker and/or a prosthetic joint. Patients with implanted pacemakers who experienced an FBR had lower survival rates than those without detectable FBR. Chronic FBR has been reported in human cochlear implants in response to their platinum electrodes and other materials, contributing to hearing loss, a reduction in the dynamic stimulation range of the device and a reduced battery life due to higher electrode impedences[162].

Approaches to reducing FBRs include mechanical matching of the device to the surrounding tissue of the host[163]; reducing the implant size and/or optimizing device geometry[160]; smooth texturing of the implant surface[127]; the incorporation of biocompatible encapsulation materials; and the delivery of anti-inflammatory drugs local to the tissue–implant interface to inhibit inflammatory activity and fibrosis[159]. Bioresorbable devices are attractive for relatively short-term or acute applications, as they naturally degrade within the body without the need for separate surgeries for device removal; they may also prevent the formation of fibrotic capsules. However, the rate of material degradation and type of by-products formed during the process of dissolution and resorption may influence the development of FBRs[164].

## Glossary

**Amperometric**
An electroanalytical technique that measures current generated by the oxidation and reduction of an electroactive biological analyte.

**Aptamer-based molecular switches**
Molecular mechanisms by which aptamers bind to the target and undergo structural conformational changes.

**Aptamer-based sensors**
A biosensor category that uses short, single-stranded DNA or RNA to specifically bind to target analytes.

**Electrochemistry**
The study of the relationship between electrical and chemical processes, often applied to biosensors for detection of target analytes.

**Impedance**
An electroanalytical technique that measures changes in the electrical impedance of an electrode surface in the presence of the target molecule.

**Interpenetrating polymer network**
Polymer chains, comprising two or more networks, that are interlaced at molecular scales.

**Iontophoresis**
An electrical technique that passes a weak electrical current through the skin to deliver ions or drugs for extraction of sweat or interstitial fluid.

**Polyaniline ink**
A highly conducting polymeric ink, frequently used for biosensing applications.

**Potentiometric**
An electroanalytical technique that measures electrical potential as an analytical signal generated by an electrochemical reaction.

**Surface-enhanced Raman scattering**
A signal amplification technique that enhances Raman scattering by surface roughness for detection of target analytes.

**Ultradian rhythms**
Biological cycles that occur with periods shorter than 24 h.

**Device operating lifetimes.** Powering devices on chronic timescales (that is, several months to decades) is a key challenge for the translation of implantable devices. Implantable devices with batteries[138] are bulky, have limited capacity, and pose a risk of rapid discharge and/or overheating and leaching of internal battery components into the body in the event of a breach of encapsulation or other device failure. In miniature devices (<1 cm in any dimension) with low-power applications and optimized electronic power consumption, batteries can operate within the bodies of small animals for several months[145]. Rechargeable batteries and accompanying wireless recharging circuitry[165] can circumvent the limited operating lifetimes of conventional non-rechargeable batteries but have the drawbacks of increased device size and the challenge of radio-frequency power attenuation in the body.

Implantable devices that are powered wirelessly through near-field communication (NFC) with thin (<1 mm) form-factors can operate effectively in small animal models and non-human primates[135,166]. However, the radio-frequency coil antennas that are required for these devices occupy considerable lateral areas. Moreover, attenuation of radio-frequency power once implanted and the requirements for alignment between the transmission antenna and receiving antenna can lead to power loss and/or insufficient power delivery to the device. In addition, this approach requires constant proximity of the patient and implanted device to an external powering antenna for continuous data collection. A 2021 study reported the development of a highly miniaturized implantable temperature sensor (<0.1 $mm^3$) powered via ultrasound[123]. The advantages of this device were its small size and its longevity, but its requirement for an external ultrasound power source represents a limitation.

In addition to power sources, selection of appropriate encapsulation materials that prevent biofluid ingress into the device and prevent FBRs are necessary to prolong the functionality of implanted devices[125]. Often, the requirements for biocompatibility, mechanical matching with surrounding tissue and fluid impenetrability represent conflicting parameters for any one encapsulation material. Layered encapsulation structures that seal or protect the internal device electronics and underlie subsequent layers that interface with the tissue may be a potential area for future exploration.

**Alternate sensing approaches.** Beyond the above-described challenges, future research in implantable devices for monitoring of kidney health should explore additional sensing approaches, including tissue mechanical properties (such as elastic modulus)[167] and/or other semi-invasive approaches to monitoring processes such as transplant rejection, as has been described for the granzyme-B sensitive nanosensor[168]. That study used an intravenously injected nanoparticle that accumulates at the site of the graft and is cleaved by granzyme B generated in the graft tissue, releasing a fluorescent indicator that is filtered by the kidney into the urine. The sensor has high sensitivity and specificity for granzyme B, which is a direct byproduct of cytotoxic T cells activated during acute rejection. Although that study involved demonstrations in skin allografts, it has potential for use in kidney allografts. Some limitations of this approach include a reliance on the kidney to filter the cleaved nanosensor (where the filtration capabilities of the kidney during renal graft rejection may be compromised); the requirement for off-site urinalysis; and a discrete 2-day measurement cycle to enable full clearance of background fluorescence from the urine. Similar to the above-described implantable thermal approaches, the device may also not be specific to allograft rejection, as granzyme B can also be produced as a result of viral infections such as BK virus.

## Conclusions

Advances in microelectronics, biosensing and microfabrication techniques form the basis of a wide range of wearable biochemical sensors and implantable electronics for health care monitoring applications, including systems that target kidney-relevant biomarkers. These platforms have strong potential to improve patient health and satisfaction by reducing the frequency of hospital visits for blood draws and by providing information on daily fluctuations in the health status of a patient. They may enhance our understanding of kidney disease at early stages as well progression to kidney failure, and may also aid the real-time identification of crucial events to facilitate pre-emptive disease intervention.

These devices are a strong focus of contemporary research, and translational opportunities for the use of wearable devices in the near term, and implantable devices in the long term, show promise for improved health care outcomes for patients with kidney disease. Future biosensing systems that integrate biosensors with advanced bioelectronic engineering schemes will likely improve the capabilities of the platforms summarized here. Examination of bio-signal variations in response to treatment may enable closed-loop operations for precision dosing. Commercial translation offers strong potential to increase overall patient well-being, to reduce costs associated with kidney monitoring and treatment, and to provide invaluable biochemical information that can improve clinical decision making in the treatment of kidney disease.

Published online: 29 April 2025

### References


1. Francis, A. et al. Chronic kidney disease and the global public health agenda: an international consensus. *Nat. Rev. Nephrol.* **20**, 473–485 (2024).
2. Webster, A. C., Nagler, E. V., Morton, R. L. & Masson, P. Chronic kidney disease. *Lancet* **389**, 1238–1252 (2017).
3. Kellum, J. A. et al. Acute kidney injury. *Nat. Rev. Dis. Primers* **7**, 52 (2021).
4. Tucker, E. L. et al. Life and expectations post-kidney transplant: a qualitative analysis of patient responses. *BMC Nephrol.* **20**, 175 (2019).
5. Giwa, S. et al. The promise of organ and tissue preservation to transform medicine. *Nat. Biotechnol.* **35**, 530–542 (2017).
6. Hariharan, S., Israni, A. K. & Danovitch, G. Long-term survival after kidney transplantation. *N. Engl. J. Med.* **385**, 729–743 (2021).
7. Delanaye, P., Cavalier, E. & Pottel, H. Serum creatinine: not so simple! *Nephron* **136**, 302–308 (2017).
8. Ostermann, M. et al. Biomarkers in acute kidney injury. *Ann. Intensive Care* **14**, 145 (2024).
9. Seki, M. et al. Blood urea nitrogen is independently associated with renal outcomes in Japanese patients with stage 3–5 chronic kidney disease: a prospective observational study. *BMC Nephrol.* **20**, 1–10 (2019).
10. Sharma, S. & Smyth, B. From proteinuria to fibrosis: an update on pathophysiology and treatment options. *Kidney Blood Press. Res.* **46**, 411–420 (2021).
11. Carrero, J. J. et al. Albuminuria changes are associated with subsequent risk of end-stage renal disease and mortality. *Kidney Int.* **91**, 244–251 (2017).
12. Menon, M. C., Murphy, B. & Heeger, P. S. Moving biomarkers toward clinical implementation in kidney transplantation. *J. Am. Soc. Nephrol.* **28**, 735–747 (2017).
13. Bloom, R. D. & Augustine, J. J. Beyond the biopsy: monitoring immune status in kidney recipients. *Clin. J. Am. Soc. Nephrol.* **16**, 1413–1422 (2021).
14. El-Bandar, N. et al. Kidney perfusion in contrast-enhanced ultrasound (CEUS) correlates with renal function in living kidney donors. *J. Clin. Med.* **11**, 791 (2022).
15. Singla, R. K., Kadatz, M., Rohling, R. & Nguan, C. Kidney ultrasound for nephrologists: a review. *Kidney Med.* **4**, 100464 (2022).
16. Thurman, J. & Gueler, F. Recent advances in renal imaging. *F1000Res* **7**, F1000 (2018).
17. Francis, S. T., Selby, N. M. & Taal, M. W. Magnetic resonance imaging to evaluate kidney structure, function, and pathology: moving toward clinical application. *Am. J. Kidney Dis.* **82**, 491–504 (2023).
18. Hull, K. L., Adenwalla, S. F., Topham, P. & Graham-Brown, M. P. Indications and considerations for kidney biopsy: an overview of clinical considerations for the non-specialist. *Clin. Med.* **22**, 34–40 (2022).
19. Schnuelle, P. Renal biopsy for diagnosis in kidney disease: indication, technique, and safety. *J. Clin. Med.* **12**, 6424 (2023).
20. Poggio, E. D. et al. Systematic review and meta-analysis of native kidney biopsy complications. *Clin. J. Am. Soc. Nephrol.* **15**, 1595–1602 (2020).

21. Bufkin, K. B., Karim, Z. A. & Silva, J. Review of the limitations of current biomarkers in acute kidney injury clinical practices. *SAGE Open. Med.* **12**, 20503121241228446 (2024).
22. Chung, H. U. et al. Binodal, wireless epidermal electronic systems with in-sensor analytics for neonatal intensive care. *Science* **363**, eaau0780 (2019).
23. Gao, W. et al. Fully integrated wearable sensor arrays for multiplexed in situ perspiration analysis. *Nature* **529**, 509–514 (2016).
24. Mickle, A. D. et al. A wireless closed-loop system for optogenetic peripheral neuromodulation. *Nature* **565**, 361–365 (2019).
25. Zhao, C., Park, J., Root, S. E. & Bao, Z. Skin-inspired soft bioelectronic materials, devices and systems. *Nat. Rev. Bioeng.* **2**, 671–690 (2024).
26. Xu, S., Kim, J., Walter, J. R., Ghaffari, R. & Rogers, J. A. Translational gaps and opportunities for medical wearables in digital health. *Sci. Transl. Med.* **14**, eabn6036 (2022).
27. Kukkar, D., Zhang, D., Jeon, B. H. & Kim, K.-H. Recent advances in wearable biosensors for non-invasive monitoring of specific metabolites and electrolytes associated with chronic kidney disease: performance evaluation and future challenges. *TrAC. Trends Anal. Chem.* **150**, 116570 (2022).
28. Tricoli, A. & Neri, G. Miniaturized bio-and chemical-sensors for point-of-care monitoring of chronic kidney diseases. *Sensors* **18**, 942 (2018).
29. Strauss, C., Booke, H., Forni, L. & Zarbock, A. Biomarkers of acute kidney injury: from discovery to the future of clinical practice. *J. Clin. Anesth.* **95**, 111458 (2024).
30. Dhondup, T. & Qian, Q. Acid-base and electrolyte disorders in patients with and without chronic kidney disease: an update. *Kidney Dis.* **3**, 136–148 (2017).
31. Tesch, G. H. Review: serum and urine biomarkers of kidney disease: a pathophysiological perspective. *Nephrology* **15**, 609–616 (2010).
32. Gowda, S. et al. Markers of renal function tests. *N. Am. J. Med. Sci.* **2**, 170–173 (2010).
33. Kim, J., Campbell, A. S., de Avila, B. E. & Wang, J. Wearable biosensors for healthcare monitoring. *Nat. Biotechnol.* **37**, 389–406 (2019).
34. Baker, L. B. Physiology of sweat gland function: the roles of sweating and sweat composition in human health. *Temperature* **6**, 211–259 (2019).
35. Zhang, Y. et al. Passive sweat collection and colorimetric analysis of biomarkers relevant to kidney disorders using a soft microfluidic system. *Lab. Chip* **19**, 1545–1555 (2019).
36. Choi, J., Ghaffari, R., Baker, L. B. & Rogers, J. A. Skin-interfaced systems for sweat collection and analytics. *Sci. Adv.* **4**, eaar3921 (2018).
37. Kim, S. B. et al. Soft, skin-interfaced microfluidic systems with wireless, battery-free electronics for digital, real-time tracking of sweat loss and electrolyte composition. *Small* **14**, e1802876 (2018).
38. Koh, A. et al. A soft, wearable microfluidic device for the capture, storage, and colorimetric sensing of sweat. *Sci. Transl. Med.* **8**, 366ra165 (2016).
39. Choi, J., Kang, D., Han, S., Kim, S. B. & Rogers, J. A. Thin, soft, skin-mounted microfluidic networks with capillary bursting valves for chrono-sampling of sweat. *Adv. Healthc. Mater.* **6**, 1601355 (2017).
40. Sempionatto, J. R. et al. An epidermal patch for the simultaneous monitoring of haemodynamic and metabolic biomarkers. *Nat. Biomed. Eng.* **5**, 737–748 (2021).
41. al-Tamer, Y. Y., Hadi, E. A. & al-Baldrani, I. I.Sweat urea, uric acid and creatinine concentrations in uraemic patients. *Urol. Res.* **25**, 337–340 (1997).
42. Yang, Y. R. et al. A laser-engraved wearable sensor for sensitive detection of uric acid and tyrosine in sweat. *Nat. Biotechnol.* **38**, 217 (2020).
43. Adelaars, S. et al. The correlation of urea and creatinine concentrations in sweat and saliva with plasma during hemodialysis: an observational cohort study. *Clin. Chem. Lab. Med.* **62**, 1118–1125 (2024).
44. Altamer, Y. Y. & Hadi, E. A. Age-dependent reference intervals of glucose, urea, protein, lactate and electrolytes in thermally-induced sweat. *Eur. J. Clin. Chem. Clin* **32**, 71–77 (1994).
45. Kwon, K. et al. An on-skin platform for wireless monitoring of flow rate, cumulative loss and temperature of sweat in real time. *Nat. Electron.* **4**, 302–312 (2021).
46. Kim, H. S. et al. Hand-held Raman spectrometer-based dual detection of creatinine and cortisol in human sweat using silver nanoflakes. *Anal. Chem.* **93**, 14996–15004 (2021).
47. Kalasin, S., Sangnuang, P. & Surareungchai, W. Satellite-based sensor for environmental heat-stress sweat creatinine monitoring: the remote artificial intelligence-assisted epidermal wearable sensing for health evaluation. *ACS Biomater. Sci. Eng.* **7**, 322–334 (2021).
48. Kalasin, S. & Sangnuang, P. Multiplex wearable electrochemical sensors fabricated from sodiated polymers and mxene nanosheet to measure sodium and creatinine levels in sweat. *ACS Appl. Nano Mater.* **6**, 18209–18221 (2023).
49. Rakesh Kumar, R. K., Shaikh, M. O. & Chuang, C. H. A review of recent advances in non-enzymatic electrochemical creatinine biosensing. *Anal. Chim. Acta* **1183**, 338748 (2021).
50. Hussain, S. & Park, S. Y. Sweat-based noninvasive skin-patchable urea biosensors with photonic interpenetrating polymer network films integrated into PDMS chips. *Acs Sens.* **5**, 3988–3998 (2020).
51. Promphet, N. et al. Cotton thread-based wearable sensor for non-invasive simultaneous diagnosis of diabetes and kidney failure. *Sens. Actuators B: Chem.* **321**, 128549 (2020).
52. Singh, S., Sharma, M. & Singh, G. Recent advancements in urea biosensors for biomedical applications. *IET Nanobiotechnol.* **15**, 358–379 (2021).
53. Ibáñez-Redín, G. et al. Wearable potentiometric biosensor for analysis of urea in sweat. *Biosens. Bioelectron.* **223**, 114994 (2023).
54. Liu, Y. L. et al. Flexible electrochemical urea sensor based on surface molecularly imprinted nanotubes for detection of human sweat. *Anal. Chem.* **90**, 13081–13087 (2018).
55. Xu, Z. Y. et al. A conducting polymer PEDOT:PSS hydrogel based wearable sensor for accurate uric acid detection in human sweat. *Sens. Actuators B: Chem.* **348**, 130674 (2021).
56. Huang, C. T., Chen, M. L., Huang, L. L. & Mao, I. F. Uric acid and urea in human sweat. *Chin. J. Physiol.* **45**, 109–115 (2002).
57. Pirovano, P. et al. A wearable sensor for the detection of sodium and potassium in human sweat during exercise. *Talanta* **219**, 121145 (2020).
58. Yuan, Z. et al. A multi-modal sweat sensing patch for cross-verification of sweat rate, total ionic charge, and $Na^+$ concentration. *Lab. Chip* **19**, 3179–3189 (2019).
59. Nyein, H. Y. Y. et al. A wearable microfluidic sensing patch for dynamic sweat secretion analysis. *ACS Sens.* **3**, 944–952 (2018).
60. Alizadeh, A. et al. A wearable patch for continuous monitoring of sweat electrolytes during exertion. *Lab. Chip* **18**, 2632–2641 (2018).
61. Parrilla, M. et al. Wearable potentiometric ion patch for on-body electrolyte monitoring in sweat: toward a validation strategy to ensure physiological relevance. *Anal. Chem.* **91**, 8644–8651 (2019).
62. Friedel, M. et al. Opportunities and challenges in the diagnostic utility of dermal interstitial fluid. *Nat. Biomed. Eng.* **7**, 1541–1555 (2023).
63. Xu, N. et al. Microneedle-based technology: toward minimally invasive disease diagnostics. *Adv. Mater. Technol-Us* **7**, 2101595 (2022).
64. Zheng, H. et al. Reverse iontophoresis with the development of flexible electronics: a review. *Biosens. Bioelectron.* **223**, 115036 (2023).
65. Metry, G. S., Attman, P. O., Lonnroth, P., Beshara, S. N. & Aurell, M. Urea kinetics during hemodialysis measured by microdialysis-a novel technique. *Kidney Int.* **44**, 622–629 (1993).
66. Wascotte, V. et al. Non-invasive diagnosis and monitoring of chronic kidney disease by reverse iontophoresis of urea in vivo. *Eur. J. Pharm. Biopharm.* **69**, 1077–1082 (2008).
67. Ebah, L. M. et al. Reverse iontophoresis of urea in health and chronic kidney disease: a potential diagnostic and monitoring tool? *Eur. J. Clin. Invest.* **42**, 840–847 (2012).
68. Varadharaj, E. K. & Jampana, N. Non-invasive potentiometric sensor for measurement of blood urea in human subjects using reverse iontophoresis. *J. Electrochem. Soc.* **163**, B340 (2016).
69. Zheng, L., Zhu, D., Xiao, Y., Zheng, X. & Chen, P. Microneedle coupled epidermal sensor for multiplexed electrochemical detection of kidney disease biomarkers. *Biosens. Bioelectron.* **237**, 115506 (2023).
70. Dervisevic, M., Jara Fornerod, M. J., Harberts, J., Zangabad, P. S. & Voelcker, N. H. Wearable microneedle patch for transdermal electrochemical monitoring of urea in interstitial fluid. *ACS Sens.* **9**, 932–941 (2024).
71. Miller, P. R. et al. Microneedle-based transdermal sensor for on-chip potentiometric determination of K(+). *Adv. Healthc. Mater.* **3**, 876–881 (2014).
72. Parrilla, M. et al. Wearable all-solid-state potentiometric microneedle patch for intradermal potassium detection. *Anal. Chem.* **91**, 1578–1586 (2019).
73. Shukla, S., Machekposhti, S. A., Joshi, N., Joshi, P. & Narayan, R. J. Microneedle-integrated device for transdermal sampling and analyses of targeted biomarkers. *Small Sci.* **3**, 2200087 (2023).
74. Huang, X. S. et al. 3D-assembled microneedle ion sensor-based wearable system for the transdermal monitoring of physiological ion fluctuations. *Microsyst. Nanoeng.* **9**, 25 (2023).
75. Molinero-Fernández, A., Casanova, A., Wang, Q. Y., Cuartero, M. & Crespo, G. A. In vivo transdermal multi-ion monitoring with a potentiometric microneedle-based sensor patch. *ACS Sensors* **8**, 158–166 (2022).
76. Li, H. et al. Microneedle-based potentiometric sensing system for continuous monitoring of multiple electrolytes in skin interstitial fluids. *ACS Sens.* **6**, 2181–2190 (2021).
77. Zhu, D. D. et al. Microneedle-coupled epidermal sensors for in-situ-multiplexed ion detection in interstitial fluids. *ACS Appl. Mater. Interfaces* https://doi.org/10.1021/acsami.3c00573 (2023).
78. Zheng, Y. B. et al. A wearable microneedle-based extended gate transistor for real-time detection of sodium in interstitial fluids. *Adv. Mater.* **34**, e2108607 (2022).
79. Li, M. S. et al. Current and future perspectives on microfluidic tear analytic devices. *ACS Sens.* **7**, 1300–1314 (2022).
80. Giardini, A. & Roberts, J. R. Concentration of glucose and total chloride in tears. *Br. J. Ophthalmol.* **34**, 737–743 (1950).
81. Kang, J., Fulop, G. & Friedman, A. H. Tear urea nitrogen and creatinine levels in renal patients. *Acta Ophthalmol.* **66**, 407–412 (1988).
82. Thomas, N., Lähdesmäki, I. & Parviz, B. A. A contact lens with an integrated lactate sensor. *Sens. Actuators B: Chem.* **162**, 128–134 (2012).
83. Liu, H., Yan, X., Gu, Z., Xiu, G. & Xiao, X. Electrochemical sensing in contact lenses. *Electroanalysis* **34**, 227–236 (2021).
84. Yang, X. et al. Flexible, wearable microfluidic contact lens with capillary networks for tear diagnostics. *J. Mater. Sci.* **55**, 9551–9561 (2020).
85. Badugu, R., Szmacinski, H., Reece, E. A., Jeng, B. H. & Lakowicz, J. R. Fluorescent contact lens for continuous non-invasive measurements of sodium and chloride ion concentrations in tears. *Anal. Biochem.* **608**, 113902 (2020).
86. Moreddu, R. et al. Integration of paper microfluidic sensors into contact lenses for tear fluid analysis. *Lab. Chip* **20**, 3970–3979 (2020).
87. Moreddu, R. et al. Lab-on-a-contact lens platforms fabricated by multi-axis femtosecond laser ablation. *Small* **17**, e2102008 (2021).
88. Mukundan, G. & Badhulika, S. Nickel-cobalt metal-organic frameworks based flexible hydrogel as a wearable contact lens for electrochemical sensing of urea in tear samples. *Mikrochim. Acta* **191**, 252 (2024).

89. Lakowicz, J. R., Badugu, R., Sivashanmugan, K. & Reece, A. Remote measurements of tear electrolyte concentrations on both sides of an inserted contact lens. *Chemosensors* **11**, 463 (2023).
90. Ku, M. et al. Smart, soft contact lens for wireless immunosensing of cortisol. *Sci. Adv.* **6**, eabb2891 (2020).
91. Badugu, R., Szmacinski, H., Reece, E. A., Jeng, B. H. & Lakowicz, J. R. Sodium-sensitive contact lens for diagnostics of ocular pathologies. *Sens. Actuators B Chem.* **331**, 129434 (2021).
92. Park, J. et al. Soft, smart contact lenses with integrations of wireless circuits, glucose sensors, and displays. *Sci. Adv.* **4**, eaap9841 (2018).
93. Keum, D. H. et al. Wireless smart contact lens for diabetic diagnosis and therapy. *Sci. Adv.* **6**, eaba3252 (2020).
94. Sempionatto, J. R. et al. Eyeglasses-based tear biosensing system: non-invasive detection of alcohol, vitamins and glucose. *Biosens. Bioelectron.* **137**, 161–170 (2019).
95. Kalasin, S., Sangnuang, P. & Surareungchai, W. Lab-on-eyeglasses to monitor kidneys and strengthen vulnerable populations in pandemics: machine learning in predicting serum creatinine using tear creatinine. *Anal. Chem.* **93**, 10661–10671 (2021).
96. Xu, J., Tao, X., Liu, X. & Yang, L. Wearable eye patch biosensor for noninvasive and simultaneous detection of multiple biomarkers in human tears. *Anal. Chem.* **94**, 8659–8667 (2022).
97. Tiffany, T. O., Jansen, J. M., Burtis, C. A., Overton, J. B. & Scott, C. D. Enzymatic kinetic rate and end-point analyses of substrate, by use of a GeMSAEC fast analyzer. *Clin. Chem.* **18**, 829–840 (1972).
98. Jaffé, M. Ueber den Niederschlag, welchen Pikrinsäure in normalem Harn erzeugt und über eine neue Reaction des Kreatinins. *Biol. Chem.* **10**, 391–400 (1886).
99. Jung, D., Biggs, H., Erikson, J. & Ledyard, P. U. New colorimetric reaction for end-point, continuous-flow, and kinetic measurement of urea. *Clin. Chem.* **21**, 1136–1140 (1975).
100. Yetisen, A. K. et al. Scleral lens sensor for ocular electrolyte analysis. *Adv. Mater.* **32**, e1906762 (2020).
101. Moonla, C. et al. Lab-in-a-mouth and advanced point-of-care sensing systems: detecting bioinformation from the oral cavity and saliva. *ECS Sens. Plus* **1**, 021603 (2022).
102. Swetha, P., Balijapalli, U. & Feng, S.-P. Wireless accessing of salivary biomarkers based wearable electrochemical sensors: a mini-review. *Electrochem. Commun.* **140**, 107314 (2022).
103. Haji Mohammadi, M. et al. Saliva lab-on-a-chip biosensors: recent novel ideas and applications in disease detection. *Microchem. J.* **168**, 106506 (2021).
104. Lee, Y. et al. Wireless, intraoral hybrid electronics for real-time quantification of sodium intake toward hypertension management. *Proc. Natl Acad. Sci. USA* **115**, 5377–5382 (2018).
105. Kim, J. et al. Non-invasive mouthguard biosensor for continuous salivary monitoring of metabolites. *Analyst* **139**, 1632–1636 (2014).
106. Kim, J. et al. Wearable salivary uric acid mouthguard biosensor with integrated wireless electronics. *Biosens. Bioelectron.* **74**, 1061–1068 (2015).
107. Lim, H. R. et al. Smart bioelectronic pacifier for real-time continuous monitoring of salivary electrolytes. *Biosens. Bioelectron.* **210**, 114329 (2022).
108. Temilola, D. O. et al. Salivary creatinine as a diagnostic tool for evaluating patients with chronic kidney disease. *BMC Nephrol.* **20**, 387 (2019).
109. Bilancio, G. et al. Saliva for assessing creatinine, uric acid, and potassium in nephropathic patients. *BMC Nephrol.* **20**, 242 (2019).
110. Soni, A., Surana, R. K. & Jha, S. K. Smartphone based optical biosensor for the detection of urea in saliva. *Sens. Actuators B: Chem.* **269**, 346–353 (2018).
111. Labat, C. et al. Differential associations for salivary sodium, potassium, calcium, and phosphate levels with carotid intima media thickness, heart rate, and arterial stiffness. *Dis. Markers* **2018**, 3152146 (2018).
112. Kallapur, B. et al. Quantitative estimation of sodium, potassium and total protein in saliva of diabetic smokers and nonsmokers: a novel study. *J. Nat. Sci. Biol. Med.* **4**, 341–345 (2013).
113. Holden, B. A., Sweeney, D. F., Vannas, A., Nilsson, K. T. & Efron, N. Effects of long-term extended contact lens wear on the human cornea. *Invest. Ophthalmol. Vis. Sci.* **26**, 1489–1501 (1985).
114. Ghaffari, R., Rogers, J. A. & Ray, T. R. Recent progress, challenges, and opportunities for wearable biochemical sensors for sweat analysis. *Sens. Actuators B Chem.* **332**, 129447 (2021).
115. Cho, S. et al. A skin-interfaced microfluidic platform supports dynamic sweat biochemical analysis during human exercise. *Sci. Transl. Med.* **16**, eado5366 (2024).
116. Zargartalebi, H. et al. Active-reset protein sensors enable continuous in vivo monitoring of inflammation. *Science* **386**, 1146–1153 (2024).
117. Thompson, I. A. P. et al. An antibody-based molecular switch for continuous small-molecule biosensing. *Sci. Adv.* **9**, eadh4978 (2023).
118. Hariri, A. A. et al. Modular aptamer switches for the continuous optical detection of small-molecule analytes in complex media. *Adv. Mater.* **36**, e2304410 (2024).
119. Poudineh, M. et al. A fluorescence sandwich immunoassay for the real-time continuous detection of glucose and insulin in live animals. *Nat. Biomed. Eng.* **5**, 53–63 (2021).
120. Pinto, M. & Dobson, S. BK and JC virus: a review. *J. Infect.* **68**, S2–S8 (2014).
121. Reploeg, M. D., Storch, G. A. & Clifford, D. B. Bk virus: a clinical review. *Clin. Infect. Dis.* **33**, 191–202 (2001).
122. Lo, D. J., Kaplan, B. & Kirk, A. D. Biomarkers for kidney transplant rejection. *Nat. Rev. Nephrol.* **10**, 215–225 (2014).
123. Shi, C. et al. Application of a sub-0.1-mm(3) implantable mote for in vivo real-time wireless temperature sensing. *Sci. Adv.* **7**, eabf6312 (2021).
124. Kang, S. K. et al. Bioresorbable silicon electronic sensors for the brain. *Nature* **530**, 71–76 (2016).
125. Mariello, M., Kim, K., Wu, K., Lacour, S. P. & Leterrier, Y. Recent advances in encapsulation of flexible bioelectronic implants: materials, technologies, and characterization methods. *Adv. Mater.* **34**, e2201129 (2022).
126. Sang, M., Kim, K., Shin, J. & Yu, K. J. Ultra-thin flexible encapsulating materials for soft bio-integrated electronics. *Adv. Sci.* **9**, e2202980 (2022).
127. Doloff, J. C. et al. The surface topography of silicone breast implants mediates the foreign body response in mice, rabbits and humans. *Nat. Biomed. Eng.* **5**, 1115–1130 (2021).
128. Guo, H. et al. Wireless implantable optical probe for continuous monitoring of oxygen saturation in flaps and organ grafts. *Nat. Commun.* **13**, 3009 (2022).
129. Zhang, H. et al. Wireless, battery-free optoelectronic systems as subdermal implants for local tissue oximetry. *Sci. Adv.* **5**, eaaw0873 (2019).
130. Humar, A. & Matas, A. J. Surgical complications after kidney transplantation. *Semin. Dial.* **18**, 505–510 (2005).
131. Salvadori, M., Rosso, G. & Bertoni, E. Update on ischemia-reperfusion injury in kidney transplantation: pathogenesis and treatment. *World J. Transpl.* **5**, 52–67 (2015).
132. Park, J., Seok, H. S., Kim, S. S. & Shin, H. Photoplethysmogram analysis and applications: an integrative review. *Front. Physiol.* **12**, 808451 (2021).
133. Traverso, G. et al. First-in-human trial of an ingestible vitals-monitoring pill. *Device* **1**, 100125 (2023).
134. Srinivasan, S. S. et al. A vibrating ingestible bioelectronic stimulator modulates gastric stretch receptors for illusory satiety. *Sci. Adv.* **9**, eadj3003 (2023).
135. Ouyang, W. et al. An implantable device for wireless monitoring of diverse physio-behavioral characteristics in freely behaving small animals and interacting groups. *Neuron* **112**, 1764–1777.e1765 (2024).
136. Lee, K. et al. Mechano-acoustic sensing of physiological processes and body motions via a soft wireless device placed at the suprasternal notch. *Nat. Biomed. Eng.* **4**, 148–158 (2020).
137. Boutry, C. M. et al. A stretchable and biodegradable strain and pressure sensor for orthopaedic application. *Nat. Electron.* **1**, 314–321 (2018).
138. Kim, J. et al. A wireless, implantable bioelectronic system for monitoring urinary bladder function following surgical recovery. *Proc. Natl Acad. Sci. USA* **121**, e2400868121 (2024).
139. Kang, S. K., Koo, J., Lee, Y. K. & Rogers, J. A. Advanced materials and devices for bioresorbable electronics. *Acc. Chem. Res.* **51**, 988–998 (2018).
140. Zhang, Y. et al. Advances in bioresorbable materials and electronics. *Chem. Rev.* **123**, 11722–11773 (2023).
141. Lu, D. et al. Implantable, wireless, self-fixing thermal sensors for continuous measurements of microvascular blood flow in flaps and organ grafts. *Biosens. Bioelectron.* **206**, 114145 (2022).
142. Madhvapathy, S. R. et al. Implantable bioelectronic systems for early detection of kidney transplant rejection. *Science* **381**, 1105–1112 (2023).
143. Madhvapathy, S. R. et al. Advanced thermal sensing techniques for characterizing the physical properties of skin. *Appl. Phys. Rev.* **9**, 041307 (2022).
144. Crawford, K. E. et al. Advanced approaches for quantitative characterization of thermal transport properties in soft materials using thin, conformable resistive sensors. *Extreme Mech. Lett.* **22**, 27–35 (2018).
145. Madhvapathy, S. R. et al. Miniaturized implantable temperature sensors for the long-term monitoring of chronic intestinal inflammation. *Nat. Biomed. Eng.* **8**, 1040–1052 (2024).
146. Pizarro, T. T. et al. SAMP1/YitFc mouse strain: a spontaneous model of Crohn's disease-like ileitis. *Inflamm. Bowel Dis.* **17**, 2566–2584 (2011).
147. Clayton, P. A., McDonald, S. P., Russ, G. R. & Chadban, S. J. Long-term outcomes after acute rejection in kidney transplant recipients: an ANZDATA analysis. *J. Am. Soc. Nephrol.* **30**, 1697–1707 (2019).
148. Singh, N., Pirsch, J. & Samaniego, M. Antibody-mediated rejection: treatment alternatives and outcomes. *Transpl. Rev.* **23**, 34–46 (2009).
149. Levitsky, J. et al. Acute rejection increases risk of graft failure and death in recent liver transplant recipients. *Clin. Gastroenterol. Hepatol.* **15**, 584–593.e582 (2017).
150. Hopkins, P. M. et al. Prospective analysis of 1,235 transbronchial lung biopsies in lung transplant recipients. *J. Heart Lung Transpl.* **21**, 1062–1067 (2002).
151. Han, Z. et al. Vitrification and nanowarming enable long-term organ cryopreservation and life-sustaining kidney transplantation in a rat model. *Nat. Commun.* **14**, 3407 (2023).
152. He, X. & Bischof, J. C. Analysis of thermal stress in cryosurgery of kidneys. *J. Biomech. Eng.* **127**, 656–661 (2005).
153. Natesan, H. et al. A micro-thermal sensor for focal therapy applications. *Sci. Rep.* **6**, 21395 (2016).
154. Sharma, A. et al. Vitrification and nanowarming of kidneys. *Adv. Sci.* **8**, e2101691 (2021).
155. O'Brien, T. J. et al. The development of a thin-filmed noninvasive tissue perfusion sensor to quantify capillary pressure occlusion of explanted organs. *IEEE Trans. Biomed. Eng.* **64**, 1631–1637 (2017).
156. Liapis, H. et al. Banff histopathological consensus criteria for preimplantation kidney biopsies. *Am. J. Transpl.* **17**, 140–150 (2017).
157. van Stralen, K. J. et al. Diagnostic methods I: sensitivity, specificity, and other measures of accuracy. *Kidney Int.* **75**, 1257–1263 (2009).
158. Hall, I. E., Doshi, M. D., Poggio, E. D. & Parikh, C. R. A comparison of alternative serum biomarkers with creatinine for predicting allograft function after kidney transplantation. *Transplantation* **91**, 48–56 (2011).

159. Barone, D. G. et al. Prevention of the foreign body response to implantable medical devices by inflammasome inhibition. *Proc. Natl Acad. Sci. USA* **119**, e2115857119 (2022).
160. Veiseh, O. et al. Size- and shape-dependent foreign body immune response to materials implanted in rodents and non-human primates. *Nat. Mater.* **14**, 643–651 (2015).
161. Kaasch, A. J. et al. Effect of clinically uninfected orthopedic implants and pacemakers/AICDs in low-risk staphylococcus aureus bloodstream infection on crude mortality rate: a post hoc analysis of a large cohort study. *Open. Forum Infect. Dis.* **6**, ofz170 (2019).
162. Jensen, M. J. et al. Cochlear implant material effects on inflammatory cell function and foreign body response. *Hear. Res.* **426**, 108597 (2022).
163. Carnicer-Lombarte, A., Chen, S. T., Malliaras, G. G. & Barone, D. G. Foreign body reaction to implanted biomaterials and its impact in nerve neuroprosthetics. *Front. Bioeng. Biotechnol.* **9**, 622524 (2021).
164. Li, C. et al. Design of biodegradable, implantable devices towards clinical translation. *Nat. Rev. Mater.* **5**, 61–81 (2020).
165. Ciatti, J. L. et al. An autonomous implantable device for the prevention of death from opioid overdose. *Sci. Adv.* **10**, eadr3567 (2024).
166. Won, S. M., Cai, L., Gutruf, P. & Rogers, J. A. Wireless and battery-free technologies for neuroengineering. *Nat. Biomed. Eng.* **7**, 405–423 (2023).
167. Liu, H. C. et al. Wearable bioadhesive ultrasound shear wave elastography. *Sci. Adv.* **10**, eadk8426 (2024).
168. Mac, Q. D. et al. Non-invasive early detection of acute transplant rejection via nanosensors of granzyme B activity. *Nat. Biomed. Eng.* **3**, 281–291 (2019).
169. Mason, P. Blood tests used to investigate liver, thyroid or kidney function and disease. *Pharm. J.* **272**, 446–448 (2004).
170. Kayashima, S. et al. Suction effusion fluid from skin and constituent analysis: new candidate for interstitial fluid. *Am. J. Physiol.* **263**, H1623–H1627 (1992).
171. Pandya, D., Nagrajappa, A. K. & Ravi, K. S. Assessment and correlation of urea and creatinine levels in saliva and serum of patients with chronic kidney disease, diabetes and hypertension- a research study. *J. Clin. Diagn. Res.* **10**, ZC58–ZC62 (2016).
172. Ebah, L., Brenchley, P., Coupes, B. & Mitra, S. A modified in vivo flow variation technique of microdialysis for sampling uremic toxins in the subcutaneous interstitial compartment. *Blood Purif.* **32**, 96–103 (2011).
173. Mendelsohn, M., Abramson, D., Senft, S., Servodidio, C. & Gamache, P. Uric acid in the aqueous humor and tears of retinoblastoma patients. *J. AAPOS* **2**, 369–371 (1998).
174. Asadi, M., Nadhum Bahjat, M. & Hosseini, M. A review on wearable sensors for sodium detection in human sweat. *Anal. Bioanal. Electrochem.* **15**, 794–814 (2023).
175. Madden, J., O'Mahony, C., Thompson, M., O'Riordan, A. & Galvin, P. Biosensing in dermal interstitial fluid using microneedle based electrochemical devices. *Sens. Biosens. Res.* **29**, 100348 (2020).
176. Van Haeringen, N. J. Clinical biochemistry of tears. *Surv. Ophthalmol.* **26**, 84–96 (1981).
177. Ray, T. R. et al. Soft, skin-interfaced sweat stickers for cystic fibrosis diagnosis and management. *Sci. Transl. Med.* **13**, eabd8109 (2021).
178. Gonçalves, A. C. et al. Chloride and sodium ion concentrations in saliva and sweat as a method to diagnose cystic fibrosis. *J. Pediatr.* **95**, 443–450 (2019).
179. Senel, M., Dervisevic, M. & Voelcker, N. H. Gold microneedles fabricated by casting of gold ink used for urea sensing. *Mater. Lett.* **243**, 50–53 (2019).
180. Chen, Y. J. et al. Microneedle patches integrated with lateral flow cassettes for blood-free chronic kidney disease point-of-care testing during a pandemic. *Biosens. Bioelectron.* **208**, 114234 (2022).

## Acknowledgements
The authors thank Tatiana Gandlin for providing the initial version of Fig. 1 and Sarena Wapnick (Northwestern University, IL, USA) for useful discussions about the contents of the manuscript prior to submission.

## Author contributions
S.R.M., S. C., Y.X., L.G., E.F., E.G. and J.A.R. wrote the paper. All authors reviewed and edited the manuscript prior to submission.

## Competing interests
The authors declare no competing interests.

## Additional information
**Supplementary information** The online version contains supplementary material available at https://doi.org/10.1038/s41581-025-00961-2.

**Peer review information** *Nature Reviews Nephrology* thanks Jonathan Himmelfarb, Sihong Wang and Wei Gao for their contribution to the peer review of this work.